

Two-dimensional dispersion of magnetostatic volume spin waves

F. J. Buijnsters,* L. J. A. van Tilburg, A. Fasolino, and M. I. Katsnelson
*Institute for Molecules and Materials, Radboud University,
 Heyendaalseweg 135, 6525 AJ Nijmegen, Netherlands*
 (Dated: February 3, 2016)

The dipolar (magnetostatic) interaction dominates the behavior of spin waves in magnetic films in the long-wavelength regime. In an in-plane magnetized film, volume modes exist with a negative group velocity (backward volume magnetostatic spin waves), in addition to the forward surface-localized mode (Damon–Eshbach). Inside the film of finite thickness L , the volume modes have a nontrivial spatial dependence, and their two-dimensional dispersion relations $\omega(\mathbf{k})$ can be calculated only numerically. We present explicit perturbative expressions for the profiles and frequencies of the volume modes, taking into account an in-plane applied field and uniaxial anisotropy, for the regimes $\|\mathbf{k}L\| \gg 1$ and $\|\mathbf{k}L\| \ll 1$, which together provide a good indication of the behavior of the modes for arbitrary wavevector \mathbf{k} . Moreover, we derive a very accurate semianalytical expression for the dispersion relation $\omega(\mathbf{k})$ of the lowest-frequency mode that is straightforward to evaluate using standard numerical routines. Our results are useful to quickly interpret and control the excitation and propagation of spin waves in (opto-)magnetic experiments.

I. INTRODUCTION

The dipolar interaction endows magnetostatic (long-wavelength) spin waves with a very peculiar dynamics. In an in-plane magnetized ferromagnetic film, their dispersion shows a strong anisotropy originating from the magnetization vector \mathbf{M}^{1-3} . Spin waves propagating through the volume of the film appear to move backwards as their group velocity is opposite to their phase velocity (backward volume magnetostatic spin-wave modes, BVMSW)⁴. Conversely, spin waves with a wavevector $\mathbf{k} \perp \mathbf{M}$ tend to localize near the surface of the film in Damon–Eshbach (DE) modes⁵, which are forward modes. The surface localization of DE modes is exponential, with a decay length inversely proportional to the perpendicular component of \mathbf{k}^4 .

While the backward volume propagation of parallel spin waves $\mathbf{k} \parallel \mathbf{M}$ is well known, in the case of perpendicular propagation $\mathbf{k} \perp \mathbf{M}$ usually only the DE modes are considered^{4,6,7}. The DE modes are the most likely to be excited by a microstrip antenna in the Damon–Eshbach geometry⁸ and show unusual features such as nonreciprocal propagation⁹. However, in a film of finite thickness, BVMSWs are not restricted to the case $\mathbf{k} \parallel \mathbf{M}$ and can exist with any (in-plane) wavevector \mathbf{k} ; in particular, perpendicularly propagating volume modes also exist and have frequencies below the DE branch^{3,10}. The BVMSW modes are, in fact, the dominant modes in optomagnetic^{11,12} experiments as in Ref. [1], where the two-dimensional profile of the initial excitation (almost homogeneous in the film thickness) can be shaped and the subsequent dynamics observed with spatial and temporal resolution.

The propagation of spin waves can only be understood if their dispersion relation is known. For exchange spin waves (wavelength small compared to the exchange length l), as well as for spin waves propagating in an ultrathin film (thin compared to l), the dispersion relations are given by fairly simple analytical expressions⁶.

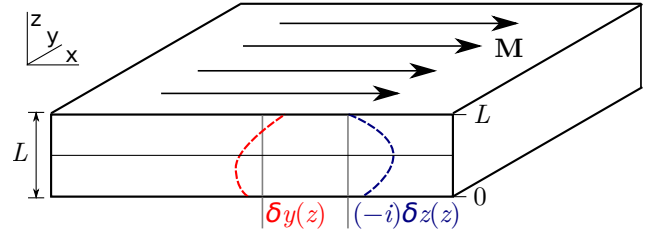


FIG. 1. (color online). Spin-wave modes in ferromagnetic films with a thickness L larger than the exchange length l have a nontrivial perpendicular profile $\delta y(z), \delta z(z)$ inside the film ($0 < z < L$). We take $\hat{\mathbf{z}}$ as the film normal and $\hat{\mathbf{x}}$ as the direction of magnetization \mathbf{M} , which is in the plane of the film. In the uniform-mode approximation, we assume that $\delta y(z)$ and $\delta z(z)$ are constant functions.

On micrometer lengthscales, however, exchange interactions are negligible and the film thickness L remains as the only characteristic lengthscale of the system. In this regime, the film can never be considered as effectively two-dimensional, and the perpendicular profile of the volume spin-wave modes, as shown in Fig. 1, is essential for an accurate description.

Because of the nontrivial profile of the mode, the true dispersion relation of the volume modes can in principle be found only numerically^{1,3}. To our knowledge, the closed-form expressions that have been derived, while useful, rely on either an effectively two-dimensional approach^{13–16} or on an artificial decoupling of Fourier components¹⁷. References [2] and [8], on the other hand, provide an analytical treatment that is in principle exact but which in practice requires the numerical solution of a set of coupled transcendental equations.

In this article, we study the dispersion and depth profile of BVMSW modes, with a particular focus on the case that $\mathbf{k} \nparallel \mathbf{M}$. The profiles of such modes show an interesting asymmetry in the perpendicular coordinate z , reminiscent of the asymmetry of the DE modes but with-

out actual surface localization^{3,17}. We derive explicit expressions for the mode profiles $\delta y(z), \delta z(z)$, up to first order in kL or $(kL)^{-1}$. Such expressions allow one, for example, to estimate to what extent the various spin-wave modes couple to an excitation homogeneous in z . We also present, in Table I, simple analytical expressions describing the asymptotic behavior of the dispersion relations of the BVMSW modes.

In addition, we present a practical and very accurate semianalytical approximation to the dispersion relation of the lowest-frequency BVMSW mode, valid on the entire \mathbf{k} plane. Our expression (62) retains the mathematical structure of an eigenvalue equation and is equivalent to the solution of a quartic polynomial equation. It can be evaluated simply and cheaply using standard numerical routines. We believe that our results are useful for a quick interpretation of experiments and for the development of new applications of directional control of optomagnetic spin-wave excitation^{1,18}.

This article is organized as follows. In Sec. II, we derive, as a first step, the spin-wave dispersion relation in the uniform-mode (effectively two-dimensional) approximation valid for ultrathin films. In Sec. III, we formulate the normal-mode problem for films of arbitrary thickness. In Sec. IV, we describe the typical behavior of the mode profiles and the dispersion relations. We successfully compare the numerical solutions to our perturbative results, which we present in detail in Sec. V. In Sec. VI, we present our semianalytical expression for the dispersion relation. Section VII provides a summary of our main conclusions.

II. UNIFORM-MODE ANALYSIS

In this section, we review the derivation of the dispersion relation of spin waves in a film in the uniform-mode approximation, where we assume that the precession amplitudes $\delta y(z), \delta z(z)$ of the magnetization inside the film do not depend on the perpendicular coordinate z . Formally, this approximation is valid only in the limit of ultrathin films ($L \ll l$). While there are some important qualitative differences between the uniform-mode expression and the dispersion relation for large film thickness L , it provides a useful first indication of the dispersion behavior of the BVMSW modes.

Specifically, taking $\hat{\mathbf{z}}$ as the film normal, we assume

$$\mathbf{M}(t, x, y, z) = M_S \mathbf{m}(t, x, y) \Pi^*\left(\frac{z}{L}\right), \quad (1)$$

where M_S is saturation magnetization, unit vector $\mathbf{m}(t, x, y)$ is the magnetization direction, and $\Pi^*(z/L)$ is the rectangular function

$$\Pi^*(z/L) = \begin{cases} 1 & \text{for } 0 < z/L < 1 \\ 0 & \text{for } z/L < 0 \text{ or } z/L > 1 \end{cases}. \quad (2)$$

In view of Sec. VD, it is convenient to define $\Pi^*(0) = \Pi^*(1) = \frac{1}{2}$.

A. Magnetostatic energy: General case

It is well known that the interaction between two magnetic point dipoles $\mathbf{v}_i, \mathbf{v}_j$ located at $\mathbf{r}_i, \mathbf{r}_j$ is given by

$$E_{\text{dip}} = -\frac{\mu_0}{4\pi} \frac{3(\mathbf{v}_i \cdot \mathbf{e}_{ij})(\mathbf{v}_j \cdot \mathbf{e}_{ij}) - \mathbf{v}_i \cdot \mathbf{v}_j}{r_{ij}^3}, \quad (3)$$

where $\mathbf{r}_{ij} = \mathbf{r}_j - \mathbf{r}_i$, $r_{ij} = \|\mathbf{r}_{ij}\|$, and $\mathbf{e}_{ij} = \mathbf{r}_{ij}/r_{ij}$. For a continuous magnetization distribution $\mathbf{M}(\mathbf{r}) = M_S \mathbf{m}(\mathbf{r})$, total energy becomes, in tensor notation,

$$\begin{aligned} E_{\text{dip}} &= \frac{1}{2} \mu_0 M_S^2 \iint m_a(\mathbf{r}') f_{ab}(\mathbf{r}' - \mathbf{r}) m_b(\mathbf{r}) d^3 r' d^3 r \\ &= \frac{1}{2} \mu_0 M_S^2 \int \tilde{m}_a^*(\mathbf{k}) \tilde{f}_{ab}(\mathbf{k}) \tilde{m}_b(\mathbf{k}) \frac{d^3 k}{(2\pi)^3}, \end{aligned} \quad (4)$$

where a, b represent the spatial directions x, y, z ; $\tilde{m}_a(\mathbf{k})$ is the Fourier transform of $m_a(\mathbf{r})$; and where we define

$$f_{ab}(\mathbf{r}) = -\frac{A_{ab}^{(2)}(\mathbf{r})}{4\pi r^5}. \quad (5)$$

The factor $1/2$ is a double-counting correction. The functions $A_{ab}^{(2)}(\mathbf{r})$ are the second-order spherical polynomials

$$A_{ab}^{(2)}(\mathbf{r}) = 3r_a r_b - \delta_{ab} r_c r_c \quad (6)$$

(eg, $A_{xx}^{(2)}(\mathbf{r}) = 3x^2 - r^2$). The Fourier transform¹⁹ of Eq. (5) is given by

$$\tilde{f}_{ab}(\mathbf{k}) = \frac{A_{ab}^{(2)}(\mathbf{k})}{3k^2}. \quad (7)$$

B. Magnetostatic energy: Uniform mode

For a magnetization profile (1) that is homogeneous in z inside the film, we have

$$\begin{aligned} E_{\text{dip}} &= \frac{1}{2} \mu_0 M_S^2 \iint m_a(\mathbf{r}') g_{ab}(\mathbf{r}' - \mathbf{r}) m_b(\mathbf{r}) d^2 r' d^2 r \\ &= \frac{1}{2} \mu_0 M_S^2 L \int \tilde{m}_a^*(\mathbf{k}) \tilde{g}_{ab}(\mathbf{k}) \tilde{m}_b(\mathbf{k}) \frac{d^2 k}{(2\pi)^2}, \end{aligned} \quad (8)$$

where

$$g_{ab}(x, y) = \frac{1}{L} \iint \Pi^*\left(\frac{z'}{L}\right) f_{ab}(x, y, z' - z) \Pi^*\left(\frac{z}{L}\right) dz' dz. \quad (9)$$

By the convolution theorem,

$$\tilde{g}_{ab}(k_x, k_y) = L \int_{-\infty}^{\infty} \tilde{f}_{ab}(k_x, k_y, k_z) \text{sinc}^2 \frac{k_z L}{2} \frac{dk_z}{2\pi}, \quad (10)$$

where we have used the Fourier transform $\tilde{\Pi}^*(kL) = e^{-ikL/2} \text{sinc}(kL/2)$ with $\text{sinc} \phi = (\sin \phi)/\phi$. We evaluate

$$\tilde{g}_{uv}(k_x, k_y) = (1 - N_k) \frac{k_u k_v}{k^2} - \frac{1}{3} \delta_{uv}, \quad (11a)$$

$$\tilde{g}_{uz}(k_x, k_y) = 0, \quad (11b)$$

$$\tilde{g}_{zz}(k_x, k_y) = N_k - \frac{1}{3}, \quad (11c)$$

where u, v represent the in-plane coordinates x, y . The demagnetizing factor N_k is given by

$$N_k = \frac{1 - e^{-kL}}{kL}. \quad (12)$$

We define $N_{k=0} = 1$ (continuity); notice that $N_{k \rightarrow \infty} = 0$.

Notice that, if we assume that the magnetization of the film is completely homogeneous ($\mathbf{k} = 0$), we get $E_{\text{dip}} = \frac{1}{2}\mu_0 M_S^2 V (-\frac{1}{3}m_x^2 - \frac{1}{3}m_y^2 + \frac{2}{3}m_z^2)$, where V is the total film volume. Due to the constraint $\|\mathbf{m}\| = 1$, this is effectively a hard-axis anisotropy of strength $\frac{1}{2}\mu_0 M_S^2$, where $\hat{\mathbf{z}}$ is the hard axis. This confirms that the dipolar interaction favors in-plane magnetization, and gives the well-known condition $K > \frac{1}{2}\mu_0 M_S^2$ for perpendicular (out-of-plane) magnetization due to an intrinsic perpendicular anisotropy K in the absence of an applied field. As a second limiting case, let us consider a system where $\mathbf{m}(x, y)$ depends only on x ($k_y = 0$) and where L is very large (thick film, $L \gg |k_x|^{-1}$). For a fixed $k_x \neq 0$, we get, in the limit $L \rightarrow \infty$, an effective local hard-axis anisotropy of strength $\frac{1}{2}\mu_0 M_S^2$, where the hard axis is $\hat{\mathbf{x}}$.

C. Linearization

In addition to the dipolar interaction, we take into account the usual micromagnetic energy functionals for exchange $E_{\text{ex}} = AL \int (\|\partial_x \mathbf{m}\|^2 + \|\partial_y \mathbf{m}\|^2) d^2r$, intrinsic easy-axis anisotropy $E_{\text{ani}} = -KL \int m_z^2 d^2r$, and Zeeman energy $E_H = -\mu_0 M_S H_x L \int m_x d^2r$. The applied field H_x fixes the equilibrium magnetization along $\hat{\mathbf{x}}$.

Linearization of the Landau–Lifshitz equation²⁰ without damping

$$\frac{\partial \mathbf{m}}{\partial t} = \frac{|\gamma|}{M_S L} \mathbf{m} \times \frac{\delta E}{\delta \mathbf{m}(\mathbf{r})} \quad (13)$$

around the equilibrium $\mathbf{m}(\mathbf{r}) = \hat{\mathbf{x}}$ gives, very generally²¹,

$$\begin{pmatrix} -\frac{\delta E}{\delta x} & -\frac{M_S L}{|\gamma|} \partial_t \\ \frac{M_S L}{|\gamma|} \partial_t & -\frac{\delta E}{\delta x} \end{pmatrix} \begin{pmatrix} \delta y \\ \delta z \end{pmatrix} + \int \left(\frac{\delta^2 E}{\delta y \delta y'} \frac{\delta^2 E}{\delta z \delta z'} \right) \begin{pmatrix} \delta y' \\ \delta z' \end{pmatrix} d^2r' = 0, \quad (14)$$

where γ is the gyromagnetic ratio and where the functional derivatives of E are to be evaluated for the equilibrium configuration $\mathbf{m}(\mathbf{r}) = \hat{\mathbf{x}}$. For brevity, we write δy for $\delta m_y(t, \mathbf{r})$ and $\delta y'$ for $\delta m_y(t, \mathbf{r}')$. The functions $\delta y, \delta z$ represent the infinitesimal deviation of magnetization \mathbf{m} from its equilibrium direction.

Substituting $E = E_{\text{ex}} + E_{\text{ani}} + E_H + E_{\text{dip}}$ and passing

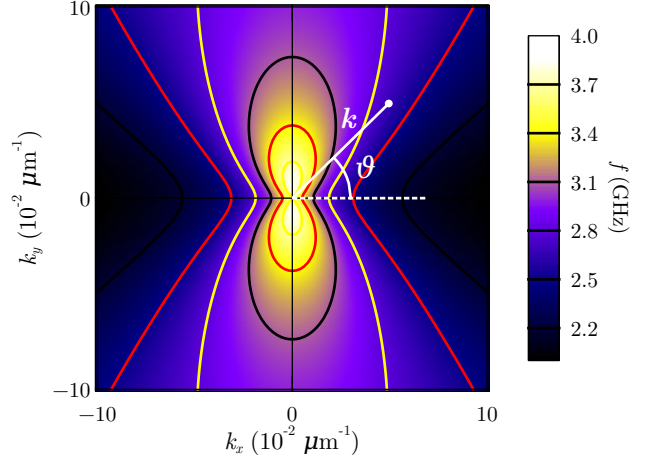


FIG. 2. (color online). Dispersion relation of BVMSWs in the uniform-mode approximation, for $H_x = 80$ kA/m, $K = 3.5$ kJ/m³, $L = 100$ μm, and $M_S = 110$ kA/m. We neglect exchange A , assuming that wavenumber k is much smaller than the inverse exchange length $1/l = \sqrt{\mu_0 M_S^2 / (2A)}$. Notice that, in the magnetostatic regime, ω (mostly) decreases in k , giving the spin waves a backward-propagating character. We define ϑ as the polar angle of the wavevector $\mathbf{k} = (k_x, k_y) = (k \cos \vartheta, k \sin \vartheta)$.

to Fourier space, Eq. (14) becomes

$$\begin{pmatrix} \frac{H_x}{M_S} + \frac{2Ak^2}{\mu_0 M_S^2} + (1 - N_k) \frac{k_y^2}{k^2} & -\frac{1}{\mu_0 |\gamma| M_S} i\omega \\ \frac{1}{\mu_0 |\gamma| M_S} i\omega & \frac{H_x}{M_S} + \frac{2Ak^2 - 2K}{\mu_0 M_S^2} + N_k \end{pmatrix} \cdot \begin{pmatrix} \widetilde{\delta y} \\ \widetilde{\delta z} \end{pmatrix} = 0, \quad (15)$$

The positive solution for ω in the characteristic equation gives the dispersion relation (*cf.* Refs. [6], [7], [22], [23])

$$\omega = |\gamma| \mu_0 \sqrt{\left[\frac{2Ak^2 - 2K}{\mu_0 M_S} + H_x + M_S N_k \right] \times \left[\frac{2Ak^2}{\mu_0 M_S} + H_x + M_S (1 - N_k) \sin^2 \vartheta \right]}, \quad (16)$$

where ϑ is the polar angle of wavevector \mathbf{k} , as shown in Fig. 2.

Figure 2 shows an example of the dispersion relation (16) for typical parameters. Notice that the dispersion relation has a cusp at the origin $\mathbf{k} = 0$. With the exception of a small area right above and below the point $\mathbf{k} = 0$, the frequency decreases with increasing k . This implies that the spin waves have a group velocity that is opposite to their wavevector k (backward modes).

III. GENERAL FORMULATION

We now turn to the general case that film thickness L is not small as compared to exchange length l , and the

dependence of the modes on the perpendicular coordinate z cannot be neglected. For simplicity, we shall, in fact, assume that both film thickness L and wavelength $2\pi/k$ are much greater than exchange length l . This allows us to neglect the exchange energy E_{ex} . In the following, whenever we refer to the short-wavelength limit $k \rightarrow \infty$, we mean the regime where the wavelength is much less than film thickness ($kL \gg 1$) but still well above the exchange length l (magnetostatic spin waves, $kl \ll 1$).

Fixing wavenumber $\mathbf{k} = (k_x, k_y)$, we allow the spin-wave mode to have an arbitrary profile $\delta y(z), \delta z(z)$ inside the film. Analogously to Eq. (15), we obtain an eigenvalue equation

$$\begin{pmatrix} H_x \hat{S} + M_S \hat{D}^{yy} & M_S \hat{D}^{yz} \\ M_S \hat{D}^{yz} & (H_x - \frac{2K}{\mu_0 M_S}) \hat{S} + M_S \hat{D}^{zz} \end{pmatrix} \begin{pmatrix} \delta y \\ \delta z \end{pmatrix} = \frac{\omega}{\mu_0 |\gamma|} \begin{pmatrix} 0 & i\hat{S} \\ -i\hat{S} & 0 \end{pmatrix} \begin{pmatrix} \delta y \\ \delta z \end{pmatrix}, \quad (17)$$

where $\delta y(z), \delta z(z)$ are now functions of z , supported on the interval $0 \leq z \leq L$. Here \hat{S} represents the identity operator. The operators \hat{D}^{ab} may be represented in Fourier space as

$$\hat{D}^{ab}(k_x, k_y) = \frac{k_a k_b}{k_x^2 + k_y^2 + k_z^2}, \quad (18)$$

where k_x, k_y should be treated as numerical constants (parameters of \hat{D}^{ab}) but k_z as an operator $\hat{k}_z = -i\partial_z$ acting on the functions $\delta y(z), \delta z(z)$.

The functions $\delta y(z), \delta z(z)$ vanish outside the interval $0 < z < L$. The finite film thickness L quantizes the modes that can be excited for any given k_y, k_z . We label the modes as $n = 1, 2, \dots$ in order of increasing $\omega > 0$.

It is convenient to normalize the solutions Ψ_+ to satisfy

$$\begin{aligned} \Psi_+^\dagger \hat{Q} \Psi_+ &= \frac{1}{\mu_0 |\gamma|} \begin{pmatrix} \delta y \\ \delta z \end{pmatrix}^\dagger \begin{pmatrix} 0 & i\hat{S} \\ -i\hat{S} & 0 \end{pmatrix} \begin{pmatrix} \delta y \\ \delta z \end{pmatrix} \\ &= \frac{2}{\mu_0 |\gamma|} \text{Im} \int_0^L \delta y(z) \delta z^*(z) dz = 1, \end{aligned} \quad (19)$$

where the asterisk denotes complex conjugation. Because the cross elements $M_S \hat{D}^{yz}$ in Eq. (17) are Hermitian, we may assume without loss of generality that $\delta y(z)$ is purely real and $\delta z(z)$ is purely imaginary. Notice that if Ψ_+ is a solution of Eq. (17) with eigenvalue ω , its complex conjugate Ψ_- is a solution with eigenvalue $-\omega$ (and norm $\Psi_-^\dagger \hat{Q} \Psi_- = -1$). The fact that solutions occur in conjugate pairs is a result of the Hamiltonianness of the normal-mode problem²¹. The negative- ω solution Ψ_- is redundant.

A. Asymptotic frequencies

Fixing the polar angle ϑ , we now turn to the behavior of Eq. (17) in the limits $k \rightarrow 0$ and $k \rightarrow \infty$ along a radial half-line (k_x, k_y) = ($k \cos \vartheta, k \sin \vartheta$).

For $k \rightarrow \infty$, the operator \hat{D}^{yy} reduces to

$$\hat{D}^{yy} = \frac{k_y^2}{k_x^2 + k_y^2 + \hat{k}_z^2} = \frac{k^2 \sin^2 \vartheta}{k^2 + \hat{k}_z^2} \rightarrow (\sin^2 \vartheta) \hat{S}, \quad (20)$$

which is a simple scalar operator; analogously, we find

$$\begin{pmatrix} \hat{D}^{yy} & \hat{D}^{yz} \\ \hat{D}^{yz} & \hat{D}^{zz} \end{pmatrix} \rightarrow \begin{pmatrix} (\sin^2 \vartheta) \hat{S} & 0 \\ 0 & 0 \end{pmatrix}. \quad (21)$$

We conclude that all modes n are degenerate in the limit $k \rightarrow \infty$, since now only the identity operator \hat{S} acts on $\delta y(z), \delta z(z)$ in Eq. (17). In particular, it follows that the uniform-mode expression (16) for ω is exact in this limit, and we have¹⁰

$$\omega_{k \rightarrow \infty} = |\gamma| \mu_0 \sqrt{\left(H_x - \frac{2K}{\mu_0 M_S}\right) \left(H_x + M_S \sin^2 \vartheta\right)}. \quad (22)$$

In the opposite limit $k \rightarrow 0$ (uniform precession), we find

$$\begin{pmatrix} \hat{D}^{yy} & \hat{D}^{yz} \\ \hat{D}^{yz} & \hat{D}^{zz} \end{pmatrix} \rightarrow \begin{pmatrix} 0 & 0 \\ 0 & \hat{S} \end{pmatrix}, \quad (23)$$

and again all modes n are degenerate; the precession frequency is given by^{10,24}

$$\omega_{k=0} = |\gamma| \mu_0 \sqrt{\left(H_x + M_S - \frac{2K}{\mu_0 M_S}\right) H_x}, \quad (24)$$

in agreement with the uniform-mode expression (16).

B. Asymptotic profiles

In the limits $k \rightarrow 0$ and $k \rightarrow \infty$, the only operator acting on the profiles $\delta y(z), \delta z(z)$ is the identity operator \hat{S} . The matrices of operators in Eq. (17) reduce to simple 2×2 scalar matrices. As a result, we can solve Eq. (17) analytically and multiply the solution vector by an arbitrary function. We obtain solutions Ψ_+ of the form

$$\Psi_0 = \begin{pmatrix} \delta y(z) \\ \delta z(z) \end{pmatrix} = \sqrt{\frac{\mu_0 |\gamma|}{2ab}} \begin{pmatrix} a \psi_0(z) \\ -ib \psi_0(z) \end{pmatrix}, \quad (25)$$

where $\psi_0(z)$ is a real-valued function supported on the interval $0 \leq z \leq L$. Notice that $\delta y(z), \delta z(z)$ differ only by a scalar factor. For the regime $k \rightarrow 0$, the values of a, b are given by

$$a = \sqrt{H_x + M_S - \frac{2K}{\mu_0 M_S}}, \quad (26a)$$

$$b = \sqrt{H_x}; \quad (26b)$$

for the regime $k \rightarrow \infty$, we have

$$a = \sqrt{H_x - \frac{2K}{\mu_0 M_S}}, \quad (27a)$$

$$b = \sqrt{H_x + M_S \sin^2 \vartheta}. \quad (27b)$$

The profile $\psi_0(z)$ must satisfy the normalization condition $\int_0^L \psi_0(z)^2 dz = 1$, but is otherwise arbitrary.

In Sec. V, we find that the degeneracy of the modes n is lifted and $\psi_0(z)$ fixed by the higher-order terms in the expansion of Eq. (17) in k or k^{-1} . For $k \rightarrow 0$, the profile $\psi_0(z)$ depends on the angle of approach ϑ^2 .

IV. MODE PROFILES AND DISPERSION

Figure 3(a) shows the dispersion relations obtained from a numerical solution of the eigenvalue equation (17). We find a sequence of modes $n = 1, 2, \dots$ that can be identified as the BVMSW modes^{2,10}. Their frequencies monotonically decrease in any direction ϑ as we move away from the origin $k = 0$. In addition, we find, for wavevectors \mathbf{k} pointing predominantly along the k_y axis (perpendicular to magnetization), a single special branch, which we identify as the DE surface mode⁵. Its frequency increases in k before leveling off to a constant value.

At $k = 0$, all modes have the same frequency $\omega_{k=0}$, given by Eq. (24). The behavior of $\omega(\mathbf{k})$ in the opposite limit $k \rightarrow \infty$ is somewhat more involved. Any given volume mode n eventually converges to the same frequency $\omega_{k \rightarrow \infty}$, given by Eq. (22), as we take $k \rightarrow \infty$. However, for any fixed wavevector \mathbf{k} , the frequency in the limit $n \rightarrow \infty$ converges to $\omega_{k=0}$. As a consequence, there is a quasicontinuum of high- n volume modes just below the line $\omega = \omega_{k=0}$.

Figure 4 shows the mode profiles $\delta y(z), \delta z(z)$ of the two lowest volume modes $n = 1, 2$ for a range of wavevectors $\mathbf{k} = (k_x, k_y) = (k \cos \vartheta, k \sin \vartheta)$. While we find that the profiles do not depend in any way on the sign of k_x , notice that the cases $k_y > 0$ and $k_y < 0$ are inequivalent². In particular, the antinode (amplitude maximum) of the $n = 1$ mode tends to move towards one or the other surface of the film ($z = 0$ or $z = L$) depending on the sign of k_y . A similar nonreciprocity is seen in the DE modes, which exponentially localize near either of the two film surfaces⁵. The explicit perturbative expressions for the mode profiles, which we present in Sec. V, can be used to quantify the asymmetric behavior.

A. Relation to uniform-mode analysis

It is interesting to compare the numerical dispersion relation of the $n = 1$ volume mode to the dispersion relation (16) obtained in the uniform-mode approximation. As shown in Fig. 3(b), we find that Eq. (16) predicts the correct group velocity $d\omega/dk$ in the $k \rightarrow 0$ limit when approaching the point $\mathbf{k} = 0$ along the k_x axis ($\vartheta = 0^\circ$ or $\vartheta = 180^\circ$). Along the k_y axis ($\vartheta = \pm 90^\circ$), however, the numerical dispersion relation differs very significantly from the uniform-mode expression. In particular, the slope $d\omega/dk$ predicted for $k \rightarrow 0$ is incorrect: we have $d\omega/dk \rightarrow 0$ for the volume modes, but Eq. (16) predicts a positive group velocity. A qualitative explanation for the

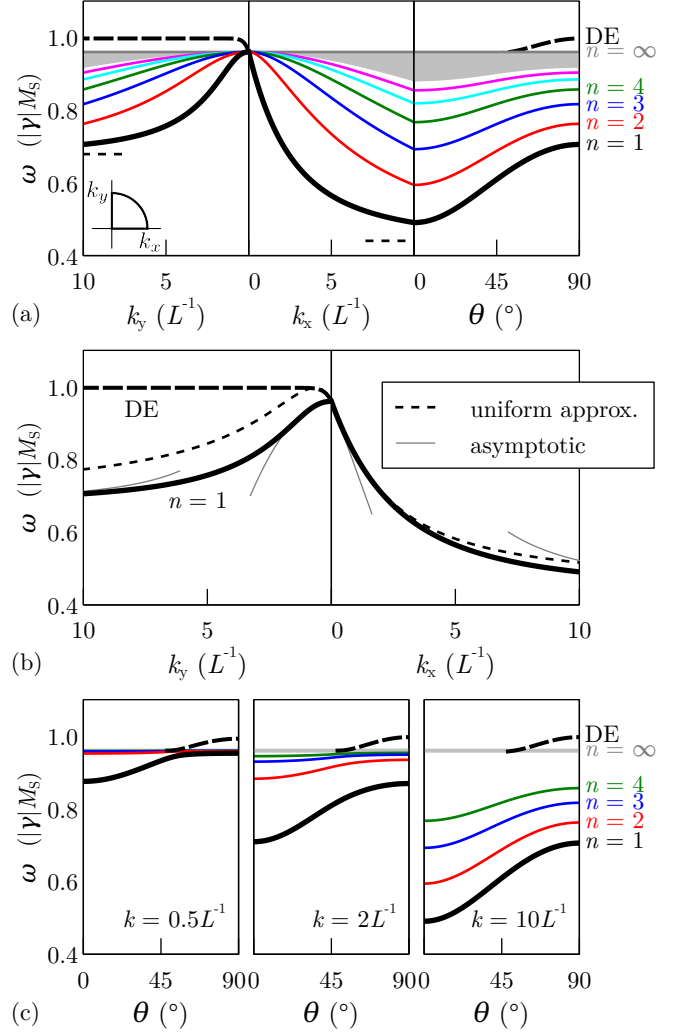


FIG. 3. (color online). (a) Numerical dispersion relations of the volume modes $n = 1, 2, \dots$ and the DE surface mode, along the k_y axis ($\vartheta = 90^\circ$), the k_x axis ($\vartheta = 0^\circ$), and a circular arc ($k = 10 L^{-1}$), taking $H_x = 0.73 M_S$ and $2K = 0.46 \mu_0 M_S^2$. For $k = 0$, all modes are degenerate, with $\omega = \omega_{k=0}$ given by Eq. (24). Taking the $k \rightarrow \infty$ limit in a fixed direction ϑ , each volume mode n eventually approaches the frequency $\omega_{k \rightarrow \infty}$ (short dotted lines), given by Eq. (22). (b) Numerical dispersion relations of the $n = 1$ and DE modes, compared to the uniform-mode expression (16). Along the k_x axis, Eq. (16) is fairly accurate, predicting the correct group velocity $d\omega/dk$ of the $n = 1$ mode for $k \rightarrow 0$. Along the k_y axis, there is a significant deviation. The correct asymptotic behavior of the $n = 1$ mode (thin solid lines) is given in Table I. (c) For small k , the crossover between the $n = 1$ and DE modes might be seen as an avoided band crossing. The behavior of the $n = 1$ mode below $\vartheta_{cr} = 49^\circ$ is similar to that of the DE mode above ϑ_{cr} , but the two modes are not continuously connected; the DE mode instead emerges from the quasicontinuum of high- n volume modes.

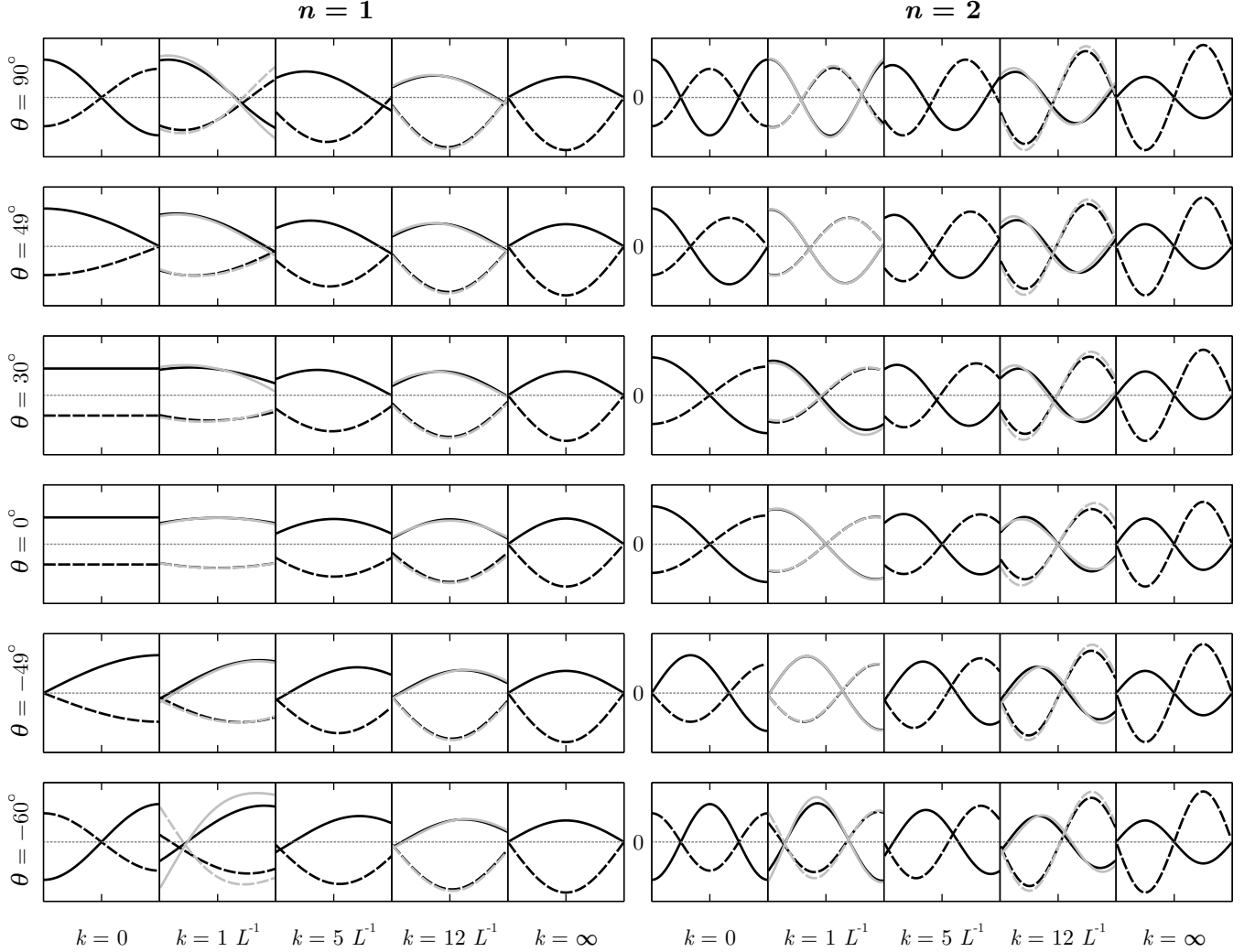


FIG. 4. Profiles $\delta y(z)$ (solid lines) and $-i\delta z(z)$ (dashed lines), with $0 \leq z \leq L$, of the lowest-frequency volume modes $n = 1, 2$, for a range of wavevectors $\mathbf{k} = (k \cos \vartheta, k \sin \vartheta)$, taking $H_x = 0.73 M_S$ and $2K = 0.46 \mu_0 M_S^2$. The modes are invariant under a reflection of \mathbf{k} with respect to the k_y axis ($\vartheta \leftrightarrow 180^\circ - \vartheta$). Notice that the limiting profile for $k = 0$ depends on the direction ϑ from which we approach the singularity at $\mathbf{k} = 0^2$. The critical angle $\vartheta_{\text{cr}} = 49^\circ$ defines the boundary between regions A (uniform limiting profile for $n = 1$) and B (sinusoidal limiting profile), as shown schematically in Fig. 5. For $k = 1 L^{-1}$ and $k = 12 L^{-1}$, we compare the numerical solutions (black lines) of the normal-mode problem (17) to the first-order approximations (gray lines) given by Eqs. (29), (31), (32), and Table II. Our first-order expressions provide a good indication of the numerical mode profiles, not only in the $k \rightarrow 0$ or $k \rightarrow \infty$ limits² but also for finite k .

discrepancy may be found in Fig. 4. Approaching $\mathbf{k} = 0$ along the k_x axis ($\vartheta = 0^\circ$), it is found² that the limiting profile $\psi_0(z)$ of the $n = 1$ mode is indeed a constant function on the interval $0 \leq z \leq L$, as was assumed in the uniform-mode approach. Along the k_y axis ($\vartheta = 90^\circ$), by contrast, we have that $\psi_0(z)$, for $0 \leq z \leq L$, is a cosine function with wavenumber π/L , and as a result, the uniform-mode analysis is inaccurate even for small k . Regardless of ϑ , the uniform-mode analysis is also inaccurate in the large- k regime (limiting profile for $k \rightarrow \infty$ is a sine function). However, the limiting frequency (22) is reproduced correctly.

Along the k_y axis, the uniform-mode dispersion rela-

tion (1) coincides, in the small- k regime, with the DE curve. The DE mode, which is exponentially localized to the surface with a decay rate proportional to k_y ⁵, assumes a uniform profile in the limit $k \rightarrow 0$. In other words, the uniform profile, which corresponds to the lowest-frequency mode ($n = 1$) for $\vartheta = 0^\circ$, becomes the highest-frequency mode (DE) for $\vartheta = 90^\circ$. At the same time, the profile of the $n = 1$ volume mode goes from uniform ($\vartheta = 0^\circ$) to sinusoidal ($\vartheta = 90^\circ$). We might interpret the transition as an avoided band crossing, as shown in Fig. 3(c). The reason for the dependence of the limiting profile $\psi_0(z)$ on ϑ is given in more formal terms in Sec. V.

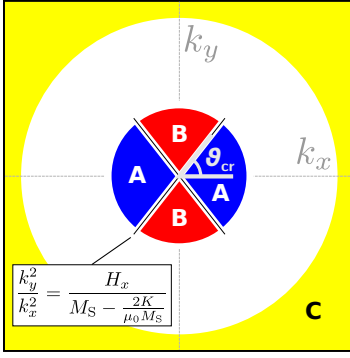


FIG. 5. (color online). Domains of applicability of the three asymptotic regimes A, B, and C. Regions A and B together represent the small- k regime. The behavior of the normal modes and frequencies is qualitatively different depending on whether one approaches the point $\mathbf{k} = 0$ from region A or region B. Region C denotes the large- k regime.

V. LIMITING BEHAVIOR

In this section, we present explicit analytical expressions for the frequency ω and profiles $\delta y(z), \delta z(z)$ of the volume modes n in the small- k and large- k regimes. While the limiting profiles for $k \rightarrow 0$ and $k \rightarrow \infty$ (zeroth order) are well known², our expressions, which are accurate up to first order in k or $1/k$, give a good impression of the behavior of the modes even for finite k , as shown in Fig. 4. They can be used to estimate how strongly each volume mode n couples to an external field pulse with a given depth profile, or to predict the contribution of the mode to net magnetization $\delta z(t, x, y) = \int \delta z(z(t, x, y, z)) dz$ as measured using Faraday rotation¹. They also describe quantitatively the asymmetry in the profiles obtained for $k_y \neq 0$. Moreover, we use the perturbation theory derived here to construct an accurate semianalytical expression for the dispersion relation of the $n = 1$ volume mode in Sec. VI.

The limiting behavior for $k \rightarrow 0$ depends essentially on the polar angle ϑ . It is useful to introduce the quantity

$$H = H_x \cos^2 \vartheta - (M_S - \frac{2K}{\mu_0 M_S}) \sin^2 \vartheta. \quad (28)$$

The boundary lines $H = 0$ separate the small- k domain into four sectors, as shown in Fig. 5. We distinguish between region A, where $H > 0$, and region B, where $H < 0$. Regions A and B meet at the critical angle $\vartheta_{\text{cr}} = \arctan \sqrt{H_x / (M_S - \frac{2K}{\mu_0 M_S})^2}$. The large- k domain is designated as region C.

It is convenient to write the mode profiles as

$$\Psi_+ = \begin{pmatrix} \delta y \\ \delta z \end{pmatrix} = \sqrt{\frac{\mu_0 |\gamma|}{2ab}} \begin{pmatrix} a [\psi(z) - \phi(z)] \\ -ib [\psi(z) + \phi(z)] \end{pmatrix}, \quad (29)$$

where $\psi(z), \phi(z)$ are real-valued functions supported on the interval $0 \leq z \leq L$. The constants $a, b > 0$ are defined by Eq. (26) for small k (regions A and B) and by Eq. (27)

for large k (region C). The normalization condition (19) becomes

$$\Psi_+^\dagger \hat{Q} \Psi_+ = \int_0^L [\psi(z)^2 - \phi(z)^2] dz = 1. \quad (30)$$

In the small- k regime (regions A and B), we expand the wavefunctions and eigenfrequencies as

$$\omega = \omega_0 + k\omega_1 + k^2\omega_2 + \dots, \quad (31a)$$

$$\psi(z) = \psi_0(z) + k\psi_1(z) + \mathcal{O}(k^2), \quad (31b)$$

$$\phi(z) = k\phi_1(z) + \mathcal{O}(k^2); \quad (31c)$$

in the large- k regime (region C), we define

$$\omega = \omega_0 + k^{-1}\omega_1 + k^{-2}\omega_2 + \dots, \quad (32a)$$

$$\psi(z) = \psi_0(z) + k^{-1}\psi_1(z) + \mathcal{O}(k^{-2}), \quad (32b)$$

$$\phi(z) = k^{-1}\phi_1(z) + \mathcal{O}(k^{-2}). \quad (32c)$$

In all three regions, only the $\psi(z)$ component of the wavefunction contributes at zeroth order ($k = 0$ or $k = \infty$); the function $\phi(z)$ vanishes in those limits [see Eq. (25)].

The main results of this section are summarized in Tables I and II, which list explicit perturbative expressions for frequency (up to second order) and profiles (up to first order) of the volume modes n , for each of the regions. For brevity, we introduce the quantities

$$A = (H_x + M_S - \frac{2K}{\mu_0 M_S}) \sin^2 \vartheta + H_x, \quad (33a)$$

$$G = H_x \cos^2 \vartheta + \frac{2K}{\mu_0 M_S} \sin^2 \vartheta, \quad (33b)$$

$$J = H_x \cos^2 \vartheta + (\frac{2K}{\mu_0 M_S} + M_S) \sin^2 \vartheta. \quad (33c)$$

The asymptotic behavior of the dispersion relations, given by the expressions in Table I, is shown for $n = 1$ in Fig. 3(b). In Fig. 4, we successfully compare our first-order mode profiles, given by the expressions in Table II, to the numerical results.

In the remainder of this section, we present in more detail the derivations for each of the regions A (Sec. V A), B (Sec. V B), and C (Sec. V D). The boundary between regions A and B, where $|\vartheta| = \vartheta_{\text{cr}}$ or $|\vartheta| = 180^\circ - \vartheta_{\text{cr}}$, requires special consideration (Sec. V C). In the interest of readability, we focus on the limiting profiles $\psi_0(z)$ of the $n = 1$ mode and on the asymptotic behavior of its dispersion relation. A more mathematical derivation of the perturbation theory used to obtain all results in Tables I and II is given in Appendix B.

A. Region A

The operators $\hat{D}^{ab}(k_x, k_y)$, defined in Eq. (18), are the only nontrivial operators appearing in the eigenvalue equation (17). We expand $\hat{D}^{ab}(k \cos \vartheta, k \sin \vartheta)$ in the pa-

TABLE I. Asymptotic behavior of the dispersion relations of the volume modes n , in each of the long-wavelength regions A, B, and the A-B boundary line and in the short-wavelength region C (see Fig. 5). The ϑ -dependent quantities H , J , and G are defined in Eqs. (28) and (33). The profiles ψ_0, ψ_1, ϕ_1 (see Table II) are shown for $n = 1$ (black lines) and $n = 2$ (gray lines).

		$\frac{\omega}{ \gamma \mu_0} = ab + \dots$	$\psi_0(z)$	$\psi_1(z)$	$\phi_1(z)$
$a = \sqrt{H_x + M_S - \frac{2K}{\mu_0 M_S}}$ $b = \sqrt{H_x}$	A ($n = 1$)	$-\frac{M_S H}{4ab} kL + \frac{M_S}{12ab} \left(J - \frac{3M_S H^2}{8a^2 b^2} \right) (kL)^2 + \mathcal{O}(k^3/H)$			
	A ($n > 1$)	$-\left(\frac{kL}{(n-1)\pi} \right)^2 \frac{M_S G}{2ab} + \mathcal{O}(k^3/H)$			
	A-B	$-\left(\frac{2kL}{(2n-1)\pi} \right)^2 \frac{M_S G_0}{2ab} q_n(\eta) + \mathcal{O}(\eta k^3 + k^3)$			
	B	$-\left(\frac{kL}{n\pi} \right)^2 \frac{M_S G}{2ab} + \mathcal{O}[k^3/(-H)]$			
$a = \sqrt{H_x - \frac{2K}{\mu_0 M_S}}$ $b = \sqrt{H_x + M_S \sin^2 \vartheta}$	C	$+\left(\frac{n\pi}{kL} \right)^2 \frac{M_S G}{2ab} + \mathcal{O}(k^{-3})$			

parameter k (for fixed ϑ). Using Appendix A, we obtain

$$\begin{aligned}
 \begin{pmatrix} \hat{D}^{yy} & \hat{D}^{yz} \\ \hat{D}^{yz} & \hat{D}^{zz} \end{pmatrix} &= \hat{D}_0 + k\hat{D}_1 + k^2\hat{D}_2 + k^3\hat{D}_3 + \dots \\
 &= \begin{pmatrix} 0 & 0 \\ 0 & \hat{S} \end{pmatrix} + k \begin{pmatrix} \pi(\sin^2 \vartheta) \delta(\hat{k}_z) & (\sin \vartheta) \hat{k}_z^{-1} \\ (\sin \vartheta) \hat{k}_z^{-1} & -\pi \delta(\hat{k}_z) \end{pmatrix} \\
 &\quad + k^2 \begin{pmatrix} (\sin^2 \vartheta) \hat{k}_z^{-2} & \pi(\sin \vartheta) \delta'(\hat{k}_z) \\ \pi(\sin \vartheta) \delta'(\hat{k}_z) & -\hat{k}_z^{-2} \end{pmatrix} \\
 &\quad + k^3 \begin{pmatrix} -\frac{1}{2} \pi(\sin^2 \vartheta) \delta''(\hat{k}_z) & -(\sin \vartheta) \hat{k}_z^{-3} \\ -(\sin \vartheta) \hat{k}_z^{-3} & \frac{1}{2} \pi \delta''(\hat{k}_z) \end{pmatrix} + \mathcal{O}(k^4),
 \end{aligned} \tag{34}$$

where δ represents the Dirac delta distribution. The expressions containing \hat{k}_z represent (in real space) convolution operators acting on the profiles $\delta y(z), \delta y(z)$; for example, the action of \hat{D}_1 may be expressed as

$$\begin{aligned}
 \hat{D}_1 \begin{pmatrix} \delta y(z) \\ \delta z(z) \end{pmatrix} &= \frac{1}{2} \times \\
 &\begin{pmatrix} \int [\sin^2 \vartheta \delta y(z') + i \sin \vartheta \text{sign}(z - z') \delta z(z')] dz' \\ \int [i \sin \vartheta \text{sign}(z - z') \delta y(z') - \delta z(z')] dz' \end{pmatrix},
 \end{aligned} \tag{35}$$

where we have used the Fourier transforms $f(z) = 1 \leftrightarrow \tilde{f}(k_z) = 2\pi\delta(k_z)$ and $f(z) = \text{sign}(z) \leftrightarrow \tilde{f}(k_z) = -2i/k_z$.

All modes n are degenerate for $k = 0$, with $\omega_0 = |\gamma|\mu_0 ab$. The first- and second-order terms of the expansion of \hat{D}^{ab} in k lift this degeneracy and fix the spatial profile $\psi_0(z)$ in Eq. (25). We obtain the profile of the

lowest mode $n = 1$ by minimizing

$$\begin{aligned}
 \omega_1 &= \Psi_0^\dagger (M_S \hat{D}_1) \Psi_0 = \\
 &= -\frac{|\gamma|\mu_0 M_S}{4ab} [H_x \cos^2 \vartheta - (M_S - \frac{2K}{\mu_0 M_S}) \sin^2 \vartheta] \\
 &\quad \times \left(\int_0^L \psi_0(z) dz \right)^2
 \end{aligned} \tag{36}$$

under the constraint $\int_0^L \psi_0(z)^2 dz = 1$ [Eq. (B14a)].

We identify the prefactor between square brackets in Eq. (36) as the quantity H . In region A ($H > 0$), minimization of ω_1 is equivalent to maximization of $(\int_0^L \psi_0(z) dz)^2$, yielding the uniform profile

$$\psi_0(z) = \frac{1}{\sqrt{L}} \Pi^* \left(\frac{z}{L} \right). \tag{37}$$

By definition, $\omega_1 = \lim_{k \rightarrow 0} d\omega/dk$ is the group velocity for $k = 0$. We obtain

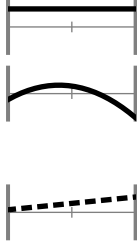
$$\frac{d\omega}{dk} = -\frac{\mu_0 |\gamma| M_S L}{4ab} H + \mathcal{O}(k), \tag{38}$$

as in the uniform-mode approach [see Fig. 3(b)].

Now that the $k = 0$ profile $\psi_0(z)$ of the $n = 1$ mode is known, the part $\phi_1(z)$ of the first-order correction is given by Eq. (B16), which condition results from minimization of ω_2 . However, the other part $\psi_1(z)$ does not affect the value of ω_2 , given by Eq. (B13c), if the constraint $\int_0^L \psi_0(z) \psi_1(z) dz = 0$ is satisfied, and hence $\psi_1(z)$ cannot be determined by minimization of ω_2 . This indeterminacy is a consequence of the degeneracy of the $\psi(z)$ component of the modes at zeroth order of perturbation theory. We turn to minimization of ω_3 to fix $\psi_1(z)$, yielding the condition (B19). The resulting profiles are listed in Table II.


TABLE II. Mode profiles and first-order corrections. All functions to be multiplied by $\Pi^*(z/L)$. See Eqs. (29), (31), (32).

Region A ($n = 1$)



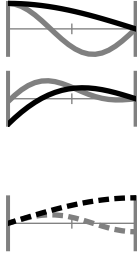
$$\begin{aligned}\psi_0(z) &= \frac{1}{\sqrt{L}} \\ \psi_1(z) &= -\frac{1}{H\sqrt{L}} \\ &\quad \times \left[\frac{AM_S \sin \vartheta}{2ab} \frac{2z-L}{2} + G \frac{3(2z-L)^2 - L^2}{12L} \right] \\ \phi_1(z) &= \frac{1}{\sqrt{L}} \frac{M_S}{2ab} \left(\frac{AL}{4ab} + \sin \vartheta \frac{2z-L}{2} \right)\end{aligned}$$

Region A ($n > 1$)



$$\begin{aligned}\psi_0(z) &= \sqrt{\frac{2}{L}} \cos\left(\frac{(n-1)\pi z}{L}\right) \\ \psi_1(z) &= -\sqrt{\frac{2}{L}} \frac{1}{H} \frac{L}{(n-1)\pi} \\ &\quad \times \left\langle \frac{AM_S \sin \vartheta}{2ab} \sin\left(\frac{(n-1)\pi z}{L}\right) \right. \\ &\quad \left. + G \left[\frac{2z-L}{L} \sin\left(\frac{(n-1)\pi z}{L}\right) \right. \right. \\ &\quad \left. \left. + \frac{1}{(n-1)\pi} \cos\left(\frac{(n-1)\pi z}{L}\right) \right] \right\rangle \\ \phi_1(z) &= \sqrt{\frac{2}{L}} \frac{M_S \sin \vartheta}{2ab} \frac{L}{(n-1)\pi} \sin\left(\frac{(n-1)\pi z}{L}\right)\end{aligned}$$


Boundary A-B (for $\eta = 0$ and $k_y > 0$)^a



$$\begin{aligned}\psi_0(z) &= \sqrt{\frac{2}{L}} \cos\left(\frac{(2n-1)\pi z}{2L}\right) \\ \psi_1(z) &= -\sqrt{\frac{2}{L}} \frac{2L}{(2n-1)\pi} \left[\frac{z-L}{L} \sin\left(\frac{(2n-1)\pi z}{2L}\right) \right. \\ &\quad \left. + \frac{1}{(2n-1)\pi} \cos\left(\frac{(2n-1)\pi z}{2L}\right) \right] \\ \phi_1(z) &= \sqrt{\frac{2}{L}} \frac{M_S}{2a^2} \frac{2L}{(2n-1)\pi} \sin\left(\frac{(2n-1)\pi z}{2L}\right)\end{aligned}$$

^a For $k_y < 0$, take $\psi_0(z) \leftarrow (-1)^{n-1} \psi_0(L-z)$ for ψ_0, ψ_1, ϕ_1 .

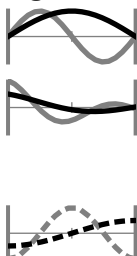
Region B^b



$$\begin{aligned}\psi_0(z) &= \pm \sqrt{\frac{2}{L}} \cos\left(\frac{n\pi z}{L}\right) \\ \psi_1(z) &= \mp \sqrt{\frac{2}{L}} \frac{1}{H} \frac{L}{n\pi} \left\langle \frac{AM_S \sin \vartheta}{2ab} \sin\left(\frac{n\pi z}{L}\right) \right. \\ &\quad \left. + G \left[\frac{2z-L}{L} \sin\left(\frac{n\pi z}{L}\right) + \frac{1}{n\pi} \cos\left(\frac{n\pi z}{L}\right) \right] \right\rangle \\ \phi_1(z) &= \sqrt{\frac{2}{L}} \frac{M_S |\sin \vartheta|}{2ab} \frac{L}{n\pi} \sin\left(\frac{n\pi z}{L}\right)\end{aligned}$$

^b For $k_y > 0$ (upper signs) and $k_y < 0$ (lower signs).

Region C



$$\begin{aligned}\psi_0(z) &= \sqrt{\frac{2}{L}} \sin\left(\frac{n\pi z}{L}\right) \\ \psi_1(z) &= \sqrt{\frac{2}{L}} \frac{1}{J} \frac{n\pi}{L} \left\langle \frac{AM_S \sin \vartheta}{2ab} \cos\left(\frac{n\pi z}{L}\right) \right. \\ &\quad \left. - G \left[\frac{2z-L}{L} \cos\left(\frac{n\pi z}{L}\right) + \frac{1}{n\pi} \sin\left(\frac{n\pi z}{L}\right) \right] \right\rangle \\ \phi_1(z) &= -\sqrt{\frac{2}{L}} \frac{M_S \sin \vartheta}{2ab} \frac{n\pi}{L} \cos\left(\frac{n\pi z}{L}\right)\end{aligned}$$

B. Region B

In region B, where $H < 0$, minimization of Eq. (36) is equivalent to minimization of $(\int_0^L \psi_0(z) dz)^2$. The minimum value

$$\omega_1 = \lim_{k \rightarrow 0} \frac{d\omega}{dk} = 0 \quad (39)$$

is obtained for any profile $\psi_0(z)$ for which $\int_0^L \psi_0(z) dz = 0$. In other words, the zeroth-order profile $\psi_0(z)$ is indeterminate even in first-order perturbation theory. The degeneracy is lifted by the second-order term of Eq. (34). By Eq. (B17), the profile $\psi_0(z)$ minimizes

$$\begin{aligned}\omega_2 &= -\frac{|\gamma| \mu_0 M_S}{2ab} [H_x \cos^2 \vartheta + \frac{2K}{\mu_0 M_S} \sin^2 \vartheta] \\ &\quad \times \int_0^L \psi_0 \hat{k}_z^{-2} \psi_0 dz. \quad (40)\end{aligned}$$

The operator \hat{k}_z^{-2} represents, as usual, a convolution in real space. Using the Fourier transform $\hat{f}(k) = k^{-n} \leftrightarrow f(x) = i(ix)^{n-1} \text{sign}(x)/[2(n-1)!]$, we have

$$\begin{aligned}\int_0^L \psi_0 \hat{k}_z^{-2} \psi_0 dz &= \\ &= -\frac{1}{2} \int_0^L \psi_0(z) \int_0^L |z-z'| \psi(z') dz' dz. \quad (41)\end{aligned}$$

Minimization of ω_2 gives

$$\psi_0(z) = \sqrt{\frac{2}{L}} \cos\left(\frac{\pi z}{L}\right) \Pi^*\left(\frac{z}{L}\right), \quad (42)$$

and we evaluate

$$\begin{aligned}\omega_2 &= \lim_{k \rightarrow 0} \frac{d\omega}{d(k^2)} = \lim_{k \rightarrow 0} \frac{1}{2k} \frac{d\omega}{dk} \\ &= -\frac{\mu_0 |\gamma| M_S L^2}{2\pi^2 ab} [H_x \cos^2 \vartheta + \frac{2K}{\mu_0 M_S} \sin^2 \vartheta]. \quad (43)\end{aligned}$$

As in region A, minimization of ω_2 immediately fixes $\phi_1(z)$ according to Eq. (B16). However, the third-order expression (B19) for $\psi_1(z)$ is indeterminate in region B. We need to minimize the fourth-order functional ω_4 , given by Eq. (B22), to determine $\psi_1(z)$. The resulting expressions are listed in Table II.

C. Boundary line A-B

The boundary line between regions A and B requires special consideration, as neither the perturbation theory of region A nor of region B is valid on this line. We find that the boundary line in some sense interpolates between the profiles in the interior of regions A and B.

On the boundary, where $H = 0$, we have that ω_1 as given by Eq. (36) is identically zero. This means that,

as in region B, the profile $\psi_0(z)$ is fixed by minimization of ω_2 . In contrast to region B, however, there is no constraint $\int_0^L \psi_0(z) dz = 0$ from minimization of ω_1 . By Eq. (B17), $\psi_0(z)$ minimizes

$$\omega_2 = -\frac{1}{2\omega_0} \int_0^L |(\hat{Y}_1^\dagger \psi_0)|^2 dz, \quad (44)$$

where

$$(\hat{Y}_1^\dagger \psi_0)(z) = -C \int_0^z \psi_0(z') dz' \quad \text{for } k_y > 0, \quad (45a)$$

$$(\hat{Y}_1^\dagger \psi_0)(z) = C \int_z^L \psi_0(z') dz' \quad \text{for } k_y < 0, \quad (45b)$$

with $C = \mu_0 |\gamma| M_S \sin \vartheta$. Minimization gives

$$\psi_0(z) = \sqrt{\frac{2}{L}} \cos\left(\frac{\pi z}{2L}\right) \Pi^*\left(\frac{z}{L}\right) \quad \text{for } k_y > 0, \quad (46a)$$

$$\psi_0(z) = \sqrt{\frac{2}{L}} \sin\left(\frac{\pi z}{2L}\right) \Pi^*\left(\frac{z}{L}\right) \quad \text{for } k_y < 0, \quad (46b)$$

and we evaluate

$$\omega_2 = \lim_{k \rightarrow 0} \frac{1}{2} \left(\frac{\partial^2 \omega}{\partial k^2} \right)_{H=0} = -|\gamma| \mu_0 \frac{4L^2}{\pi^2} \frac{M_S G_0}{2ab}, \quad (47)$$

where

$$G_0 = G|_{\vartheta=\vartheta_{\text{cr}}} = \frac{b^2 M_S}{a^2}. \quad (48)$$

Minimization of ω_2 also fixes $\phi_1(z)$ by Eq. (B16). The other first-order component $\psi_1(z)$ is again determined only at fourth order of perturbation theory.

In the above expressions, we assume that we approach the point $\mathbf{k} = 0$ along a line $H = 0$; in other words, we fix $\vartheta = \pm \vartheta_{\text{cr}}$. We can generalize Eq. (47) by carrying out the expansion along a curve of constant η , as shown in Fig. 6, where we define

$$\eta = \left(\frac{a^2}{2b^2 M_S L} \right) \frac{H}{k}. \quad (49)$$

We obtain, for the lowest mode $n = 1$,

$$\omega_2 = \lim_{k \rightarrow 0} \frac{1}{2} \left(\frac{\partial^2 \omega}{\partial k^2} \right)_\eta = -|\gamma| \mu_0 \frac{4L^2}{\pi^2} \frac{M_S G_0}{2ab} q_1(\eta). \quad (50)$$

Notice that Eq. (47) corresponds to $\eta = 0$. The generalization $\eta \neq 0$ interpolates between regions A ($\eta \rightarrow \infty$) and B ($\eta \rightarrow -\infty$) and allows one, in principle, to construct a second-order approximation of ω around $k = 0$ uniform in ϑ .

Table I gives ω_2 for arbitrary mode index n . While we are unaware of a closed-form expression for the functions $q_n(\eta)$, we have a small- k expansion

$$q_n(\eta) = 1 + 2\eta + \eta^2 - \frac{1}{6}(2n-1)^2 \pi^2 \eta^3 (1-\eta) + \mathcal{O}(\eta^5) \quad (51)$$

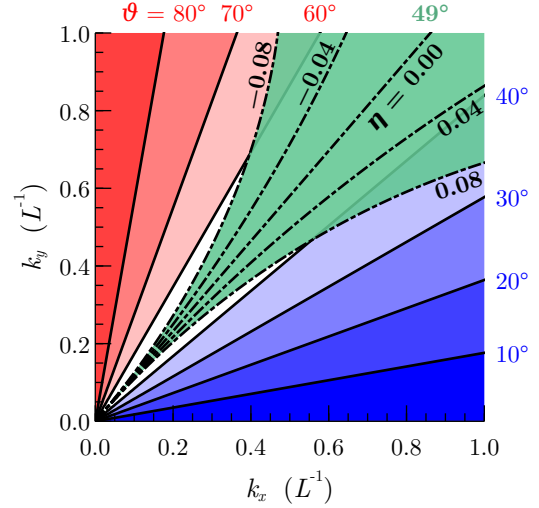


FIG. 6. (color online). In regions A (blue) and B (red), we carry out the expansion in k along lines of constant ϑ . In the A-B boundary region (green), we expand instead along curves of constant η , as defined by Eq. (49). Together, the three perturbative expressions for ω (see Table I) provide, up to the uncertainty in $q_n(\eta)$, a description of the dispersion relation that is accurate to second order in k uniformly in ϑ .

and large- k expansions

$$q_n(\eta) = \frac{\pi^2}{12} (1 + 3\eta) + \mathcal{O}(\eta^{-1}) \quad \text{for } \eta > 0, n = 1, \quad (52a)$$

$$q_n(\eta) = \left(\frac{n - \frac{1}{2}}{n - 1} \right)^2 + \mathcal{O}(\eta^{-1}) \quad \text{for } \eta > 0, n > 1, \quad (52b)$$

$$q_n(\eta) = \left(\frac{n - \frac{1}{2}}{n} \right)^2 + \mathcal{O}(-\eta^{-1}) \quad \text{for } \eta < 0. \quad (52c)$$

A very good approximation for $q_1(\eta)$, with a maximal absolute error of 0.00363, is given by

$$q_1(\eta) \approx \frac{1}{24} \left[3 + \pi^2 (1 + 3\eta) + \sqrt{[3 + \pi^2 (1 + 3\eta)]^2 - 12\pi^2 (1 + 3\eta + 3) + 432} \right]. \quad (53)$$

D. Region C

For large k , we have the expansion [cf. Eq. (34)]

$$\begin{aligned} \begin{pmatrix} \hat{D}_{yy} & \hat{D}_{yz} \\ \hat{D}_{zy} & \hat{D}_{zz} \end{pmatrix} &= \hat{D}_{-0} + k^{-1} \hat{D}_{-1} + k^{-2} \hat{D}_{-2} + \dots \\ &= \sin^2 \vartheta \begin{pmatrix} \hat{S} & 0 \\ 0 & 0 \end{pmatrix} + \frac{\sin \vartheta}{k} \begin{pmatrix} 0 & \hat{k}_z \\ \hat{k}_z & 0 \end{pmatrix} \\ &+ \frac{1}{k^2} \begin{pmatrix} -(\sin^2 \vartheta) \hat{k}_z^2 & 0 \\ 0 & \hat{k}_z^2 \end{pmatrix} - \frac{\sin \vartheta}{k^3} \begin{pmatrix} 0 & \hat{k}_z^3 \\ \hat{k}_z^3 & 0 \end{pmatrix} \\ &- \frac{1}{k^4} \begin{pmatrix} -(\sin^2 \vartheta) \hat{k}_z^4 & 0 \\ 0 & \hat{k}_z^4 \end{pmatrix} + \mathcal{O}(k^{-5}). \end{aligned} \quad (54)$$

All modes n are degenerate at zeroth order. In the $k \rightarrow \infty$ limit, the mode profiles are of the form (25) with a, b given by Eq. (27). Notice that, for region C, the value of b depends on ϑ . The second-order term \hat{D}_{-2} in Eq. (54) lifts the degeneracy and fixes the spatial profile $\psi_0(z)$.

Regardless of k_y , we have

$$\lim_{k \rightarrow \infty} -k^2 \frac{d\omega}{dk} = \omega_1 = \Psi_0^\dagger (M_S \hat{D}_{-1}) \Psi_0 = 0. \quad (55)$$

For $k_y = 0$, the first-order term \hat{D}_{-1} in Eq. (54) even vanishes identically. In this case, we may somewhat simplify our calculations by treating ω_2 as the first-order term of a perturbation series in k^2 . We find the limiting profile $\psi_0(z)$ of the $n = 1$ mode by minimization of

$$\omega_2 = \Psi_0^\dagger (M_S \hat{D}_{-2}) \Psi_0 = \frac{\mu_0 |\gamma| M_S}{2ab} H_x \int_0^L \left(\frac{d\psi_0}{dz} \right)^2 dz, \quad (56)$$

under the constraint (B14a). We obtain

$$\psi_0(z) = \sqrt{\frac{2}{L}} \sin\left(\frac{\pi z}{L}\right) \Pi^*\left(\frac{z}{L}\right) \quad (57)$$

and

$$\lim_{k \rightarrow \infty} -\frac{k^3}{2} \frac{d\omega}{dk} = \omega_2 = \mu_0 |\gamma| M_S \frac{\pi^2}{L^2} \frac{H_x}{2ab}. \quad (58)$$

Notice that $\psi_0(z)$ satisfies Dirichlet boundary conditions $\psi_0(0) = \psi_0(L) = 0$. Such conditions are necessary to give Eq. (56) a finite value, since $\psi_0(z)$ must vanish outside the interval $0 \leq z \leq L$. However, higher-order terms $\phi_1(z), \psi_1(z)$ of the expansion can have finite values for $z = 0$ or $z = L$.

In the general case $k_y \neq 0$, the profile $\psi_0(z)$ is still a sine function (57). Using Eq. (B17), we evaluate

$$\omega_2 = \frac{\mu_0 |\gamma| M_S G}{2ab} \int_0^L \left(\frac{d\psi}{dz} \right)^2 dz = \mu_0 |\gamma| M_S \frac{\pi^2}{L^2} \frac{G}{2ab}. \quad (59)$$

The profile $\phi_1(z)$ is fixed by Eq. (B16). The other first-order profile $\psi_1(z)$ is determined, again, only by minimization of the fourth-order functional ω_4 [Eq. (B22)]. Table II lists the resulting expressions.

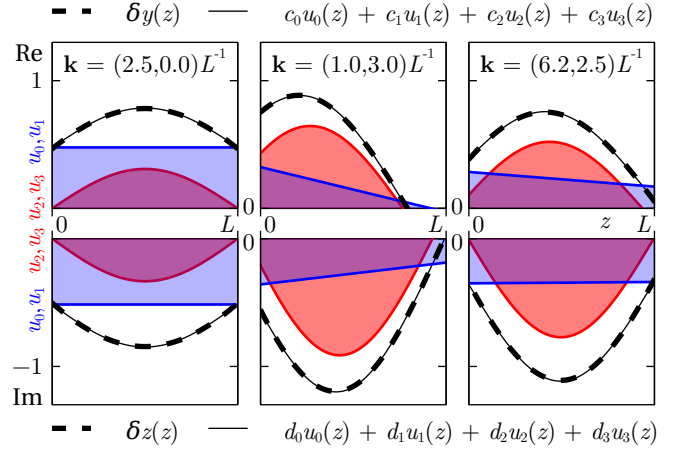


FIG. 7. (color online). Mode profiles $\delta y(z), \delta z(z)$ of the lowest-frequency mode ($n = 1$) and their approximate representations as linear combinations (61) of the basis functions u_0, u_1, u_2, u_3 , for three wavevectors $\mathbf{k} = (k_x, k_y)$, taking $H_x = 0.73 M_S$ and $2K = 0.46 \mu_0 M_S^2$. There is no visible difference between the full profiles and the approximations.

When performing the derivation of the profile $\psi_1(z)$, we take into account the following. Writing out Eqs. (B18) and (B22) for region C, we find that the functionals ω_3 and ω_4 contain terms such as $i \int \psi_1 \hat{k}_z \phi_1 dz = \int \psi_1 \partial_z \phi_1 dz$ or $\int \psi_0 \hat{k}_z^4 \psi_0 dz = \int \psi_0 \partial_z^4 \psi_0 dz$, which must be regularized; indeed, the profiles $\phi_0(z), \psi_1(z)$ have discontinuities at $z = 0$ and $z = L$, while $\psi_0(z)$ has discontinuities in its first derivative. The functionals ω_3, ω_4 can each be written as a sum of regular integral terms plus boundary terms of the forms (a) $\lim_{\Delta \rightarrow 0^+} \int_{-\Delta}^{\Delta} \Theta(z) \delta(z) dz$ and (b) $\lim_{\Delta \rightarrow 0^+} \int_{-\Delta}^{\Delta} \Theta(z) \delta'(z) dz$, where $\Theta(z)$ is the Heaviside step function. It is natural to assign the value $\frac{1}{2}$ to (a). As for terms (b), which diverge, we must require that the sum of their prefactors vanishes, yielding a boundary condition that acts as a constraint in the minimization of ω_4 .

VI. SEMIANALYTICAL SOLUTION

In this section, we present a semianalytical expression for the dispersion relation of the $n = 1$ BVMSW mode that can be evaluated in constant time using standard numerical routines. The expression is accurate up to an error that is negligible for any practical purpose (well below 0.01% in the example of Fig. 8). It takes a given wavevector (k_x, k_y) as input; evaluation does not require an initial guess for ω .

Figure 7 shows that typical profiles $\delta y(z), \delta z(z)$ of the $n = 1$ mode can be written, to a very reasonable approximation, as a linear combination of only four basis

functions

$$u_0(z) = \Pi^*\left(\frac{z}{L}\right), \quad (60a)$$

$$u_1(z) = \left(\frac{z}{L} - \frac{1}{2}\right)\Pi^*\left(\frac{z}{L}\right), \quad (60b)$$

$$u_2(z) = \sin\left(\frac{\pi z}{L}\right)\Pi^*\left(\frac{z}{L}\right), \quad (60c)$$

$$u_3(z) = -\cos\left(\frac{\pi z}{L}\right)\Pi^*\left(\frac{z}{L}\right). \quad (60d)$$

For our semianalytical approximation, we restrict the profiles to such linear combinations

$$\delta y(z) = c_0 u_0(z) + c_1 u_1(z) + c_2 u_2(z) + c_3 u_3(z), \quad (61a)$$

$$\delta z(z) = d_0 u_0(z) + d_1 u_1(z) + d_2 u_2(z) + d_3 u_3(z). \quad (61b)$$

On this basis set, the operators \hat{S} , \hat{D}^{yy} , \hat{D}^{yz} , \hat{D}^{zz} reduce to simple 4×4 matrix blocks, given below, and Eq. (17) becomes an 8×8 eigenvalue problem

$$\begin{bmatrix} H_x S + M_S D^{yy} & M_S D^{yz} \\ M_S D^{yz} & (H_x - \frac{2K}{\mu_0 M_S})S + M_S D^{zz} \end{bmatrix} v = \frac{\omega}{\mu_0 |\gamma|} \begin{bmatrix} 0 & iS \\ -iS & 0 \end{bmatrix} v, \quad (62)$$

where square brackets indicate block matrices and $v = (c_0, c_1, c_2, c_3, d_0, d_1, d_2, d_3)^T$ represents the eigenvector. The approximate frequency of the $n = 1$ mode is given by the lowest positive eigenvalue ω .

Equation (62) takes the form of an 8×8 generalized Hermitian eigenvalue problem, the solutions ω of which can be found numerically using standard routines. While not all linear-algebra computer packages may support the generalized format $Hv = \omega Qv$, it can always be rewritten as $Q^{-1}Hv = \omega v$ and solved as an ordinary non-Hermitian eigenvalue problem.

Explicit analytical expressions exist for all matrix elements in Eq. (62). The identity operator \hat{S} becomes the overlap matrix

$$S = L \begin{pmatrix} 1 & 0 & \frac{2}{\pi} & 0 \\ 0 & \frac{1}{12} & 0 & \frac{2}{\pi^2} \\ \frac{2}{\pi} & 0 & \frac{1}{2} & 0 \\ 0 & \frac{2}{\pi^2} & 0 & \frac{1}{2} \end{pmatrix}, \quad (63)$$

where the matrix elements are defined by $S_{ij} = \int u_i(z)u_j(z)dz$. The elements of the D^{ab} matrix blocks can be evaluated in Fourier space as

$$D_{ij}^{yy}(k_x, k_y) = \frac{1}{2\pi} \int \tilde{u}_i^*(k_z) \frac{k_y k_y}{k_x^2 + k_y^2 + k_z^2} \tilde{u}_j(k_z) dk_z, \quad (64)$$

and analogously for D_{ij}^{yz} and D_{ij}^{zz} , where $\tilde{u}_i(k_z)$ is the

Fourier transform of the basis function $u_i(z)$. We obtain

$$D^{yy} = L \frac{k_y^2}{k^2} \times \begin{pmatrix} 1 - N_{00} & 0 & \frac{2}{\pi}(1 - N_{02}) & 0 \\ 0 & \frac{1}{12}(1 - N_{11}) & 0 & \frac{2}{\pi^2}(1 - N_{13}) \\ \frac{2}{\pi}(1 - N_{02}) & 0 & \frac{1}{2}(1 - N_{22}) & 0 \\ 0 & \frac{2}{\pi^2}(1 - N_{13}) & 0 & \frac{1}{2}(1 - N_{33}) \end{pmatrix} \quad (65)$$

and

$$D^{zz} = L \begin{pmatrix} N_{00} & 0 & \frac{2}{\pi}N_{02} & 0 \\ 0 & \frac{1}{12}N_{11} & 0 & \frac{2}{\pi^2}N_{13} \\ \frac{2}{\pi}N_{02} & 0 & \frac{1}{2}N_{22} & 0 \\ 0 & \frac{2}{\pi^2}N_{13} & 0 & \frac{1}{2}N_{33} \end{pmatrix}, \quad (66)$$

where

$$N_{00} = \frac{1 - e^{-kL}}{kL}, \quad (67a)$$

$$N_{11} = 12 \left[\frac{1 + e^{-kL}}{4kL} + \frac{(1 + kL)e^{-kL} - 1}{k^3 L^3} \right], \quad (67b)$$

$$N_{22} = \frac{\pi^2}{k^2 L^2 + \pi^2} - \frac{2\pi^2 kL(1 + e^{-kL})}{(k^2 L^2 + \pi^2)^2}, \quad (67c)$$

$$N_{33} = \frac{\pi^2}{k^2 L^2 + \pi^2} + \frac{2k^3 L^3(1 + e^{-kL})}{(k^2 L^2 + \pi^2)^2}, \quad (67d)$$

$$N_{02} = \frac{\pi^2}{k^2 L^2 + \pi^2} \frac{1 + e^{-kL}}{2}, \quad (67e)$$

$$N_{13} = \frac{\pi^2}{k^2 L^2 + \pi^2} \frac{(1 + e^{-kL})(2 + kL)}{4} \quad (67f)$$

are the so-called demagnetizing factors; and we obtain

$$D^{yz} = \frac{k_y L^2}{2\pi i} \begin{pmatrix} 0 & \frac{\pi}{6}Z_{01} & 0 & \frac{2}{\pi}Z_{03} \\ -\frac{\pi}{6}Z_{01} & 0 & -\frac{4}{\pi^2}Z_{21} & 0 \\ 0 & \frac{4}{\pi^2}Z_{21} & 0 & Z_{23} \\ -\frac{2}{\pi}Z_{03} & 0 & -Z_{23} & 0 \end{pmatrix}, \quad (68)$$

where

$$Z_{01} = \frac{e^{-kL} + 1 - 2N_{00}}{\frac{1}{6}k^2 L^2}, \quad (69a)$$

$$Z_{03} = N_{02}, \quad (69b)$$

$$Z_{21} = \frac{\pi^2}{k^2 L^2 + \pi^2} \left(1 - \frac{\pi}{4}Z_{01}kL\right), \quad (69c)$$

$$Z_{23} = N_{22}. \quad (69d)$$

Notice that the basis set (60) has been chosen in such a way that it can represent exactly the profiles $\psi_0(z)$, $\phi_1(z)$ of the $n = 1$ mode in each of the regions A, B, and C (see Table II). As a result, we have at least second-order accuracy of ω in k or $1/k$ in those regions, as shown in Fig. 8. Since the mode profile $\psi_1(z)$ is fixed only at third (or, in regions B and C, fourth) order of perturbation

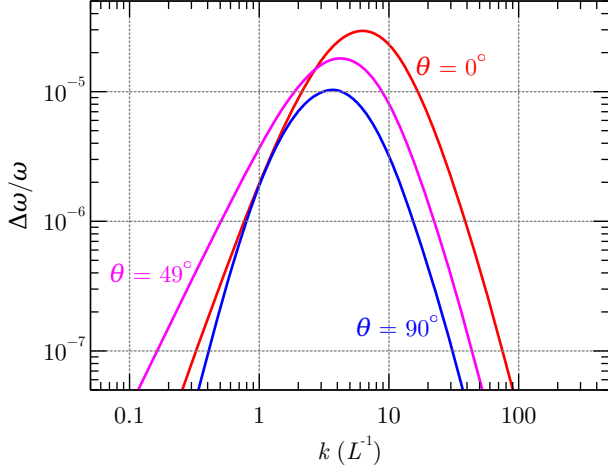


FIG. 8. (color online). Relative error $\Delta\omega/\omega$ of the semianalytical expression (62) for the dispersion relation $\omega(k \cos \vartheta, k \sin \vartheta)$, along three radials $\vartheta = 0^\circ$ (region A), $\vartheta = 90^\circ$ (region B), and $\vartheta = \vartheta_{\text{cr}} = 49^\circ$ (A-B boundary), as compared to converged solutions of the full eigenvalue problem (17) for $H_x = 0.73 M_S$ and $2K = 0.46 \mu_0 M_S^2$. In the interior of region A, we have second-order accuracy in k [$\Delta\omega = \mathcal{O}(k^3)$]; for region B, third-order accuracy [$\Delta\omega = \mathcal{O}(k^4)$]; in region C, third-order accuracy in k^{-1} [$\Delta\omega = \mathcal{O}(k^{-4})$]. On the A-B boundary line, we have only first-order accuracy [$\Delta\omega = \mathcal{O}(k^2)$]. However, the relative error remains very small on the entire domain (well below 10^{-4}).

theory (see Sec. V), it does not need to be included in the basis set to obtain second-order accuracy.

On the boundary line between regions A and B ($\vartheta = \vartheta_{\text{cr}}$), we have only first-order accuracy, because the corresponding profiles $\psi_0(z), \phi_1(z)$ are not represented in the basis set. Figure 8 shows that the error $\Delta\omega$ nonetheless remains very small. The exact small- k behavior of ω on the A-B boundary is given in Sec. VC.

We comment on our claim that the approximate expression for $\omega(k_x, k_y)$ can be evaluated in constant time. In general, the solution of an eigenvalue problem for matrices of size 5×5 or larger requires the use of iterative methods, the convergence rate of which may depend on system parameters. In our case, the characteristic equation $\text{Det}(H - \omega Q) = 0$ of the eigenvalue problem (62) contains only even powers of ω , since all eigenvalues appear in conjugate pairs (Hamiltonian problem²¹). We could therefore write the characteristic equation, a polynomial of eighth degree in ω , as a quartic polynomial in ω^2 , which can be explicitly solved by radicals. This guarantees the existence of an analytical expression for ω in principle.

VII. CONCLUSIONS

BVMSWs in magnetic films display unusual and highly nontrivial dispersion behavior. Their strongly

anisotropic and nonreciprocal propagation means that they can be excited and manipulated with a great deal of flexibility and control¹. Their specific dispersion characteristics are an important ingredient in the analysis of all-optical excitation^{25,26} and nonlinear effects^{18,27,28}.

Since the defining equations of the BVMSW modes can be solved only numerically, we believe that it is useful to have some approximate analytical results describing their essential features. In Table I, we summarize the simple analytical expressions that we have derived for the mode frequencies in the short-wavelength and long-wavelength regimes, including the behavior for wavevectors \mathbf{k} pointing in a direction close to the critical angle ϑ_{cr} . We have also obtained explicit first-order expressions for the depth profiles $\delta y(z), \delta z(z)$ of the modes, given by Eqs. (29), (31), (32), and Table II. These expressions highlight and quantify the asymmetry in z found for $k_y \neq 0$ (nonreciprocal behavior).

In addition to the perturbative results, we provide a semianalytical expression for the dispersion relation of the lowest mode $n = 1$ valid for arbitrary wavevector (k_x, k_y) . While this expression is, strictly speaking, an approximation, we find that the error is so small as to be negligible for practical purposes. The semianalytical expression is straightforward to implement using standard numerical routines.

Appendix A: Distributional limits

This appendix provides some elementary results needed to carry out the small- k expansion (34). If we set $(k_x, k_y) = (k \cos \vartheta, k \sin \vartheta)$, the operators $\hat{D}^{yy}, \hat{D}^{yz}, \hat{D}^{zz}$, defined by Eq. (18), become

$$\hat{D}^{yy} = \frac{k^2}{k^2 + \hat{k}_z^2} \sin^2 \vartheta, \quad (\text{A1a})$$

$$\hat{D}^{yz} = \frac{k \hat{k}_z}{k^2 + \hat{k}_z^2} \sin \vartheta, \quad (\text{A1b})$$

$$\hat{D}^{zz} = \frac{\hat{k}_z^2}{k^2 + \hat{k}_z^2} = \hat{S} - \frac{k^2}{k^2 + \hat{k}_z^2}. \quad (\text{A1c})$$

Equation (34) is obtained by expanding the operators $k^2/(k^2 + \hat{k}_z^2)$ and $k \hat{k}_z/(k^2 + \hat{k}_z^2)$ as a Taylor series in the parameter $k > 0$. In the following, \hat{k}_z may be substituted for x and k for ε .

We consider the expressions $\varepsilon^2/(x^2 + \varepsilon^2)$ and $\varepsilon x/(x^2 + \varepsilon^2)$ as functions of x and calculate derivatives with respect to the parameter ε in the limit $\varepsilon \rightarrow 0^+$. Most of these limits can only be defined if we turn to generalized functions (distributions) of x . We obtain

$$\lim_{\varepsilon \rightarrow 0^+} \frac{\varepsilon^2}{x^2 + \varepsilon^2} = 0, \quad (\text{A2a})$$

$$\lim_{\varepsilon \rightarrow 0^+} \frac{\varepsilon x}{x^2 + \varepsilon^2} = 0; \quad (\text{A2b})$$

$$\lim_{\varepsilon \rightarrow 0^+} \frac{\partial}{\partial \varepsilon} \frac{\varepsilon^2}{x^2 + \varepsilon^2} = \pi \delta(x), \quad (\text{A3a})$$

$$\lim_{\varepsilon \rightarrow 0^+} \frac{\partial}{\partial \varepsilon} \frac{\varepsilon x}{x^2 + \varepsilon^2} = \frac{1}{x}, \quad (\text{A3b})$$

where $\delta(x)$ is the Dirac delta distribution;

$$\lim_{\varepsilon \rightarrow 0^+} \frac{\partial^2}{\partial \varepsilon^2} \frac{\varepsilon^2}{x^2 + \varepsilon^2} = \frac{2}{x^2}, \quad (\text{A4a})$$

$$\lim_{\varepsilon \rightarrow 0^+} \frac{\partial^2}{\partial \varepsilon^2} \frac{\varepsilon x}{x^2 + \varepsilon^2} = 2\pi \delta'(x); \quad (\text{A4b})$$

and

$$\lim_{\varepsilon \rightarrow 0^+} \frac{\partial^3}{\partial \varepsilon^3} \frac{\varepsilon^2}{x^2 + \varepsilon^2} = -3\pi \delta''(x), \quad (\text{A5a})$$

$$\lim_{\varepsilon \rightarrow 0^+} \frac{\partial^3}{\partial \varepsilon^3} \frac{\varepsilon x}{x^2 + \varepsilon^2} = -\frac{6}{x^3}. \quad (\text{A5b})$$

Expressions of the form $1/x^n$ are formally defined as distributional derivatives $\frac{(-1)^{n-1}}{(n-1)!} \frac{d^n}{dx^n} \log|x|$.

Appendix B: Perturbation theory

The generalized Hermitian eigenvalue problem

$$H\Psi = \omega Q\Psi, \quad (\text{B1})$$

where H and Q are Hermitian operators one of which is positive definite, can be cast as a problem of minimization of the functional

$$\omega = \Psi^\dagger H \Psi \quad (\text{B2})$$

under the constraint

$$\Psi^\dagger Q \Psi = 1. \quad (\text{B3})$$

We suppose that H depends on a parameter k and expand the solution Ψ around $k = 0$. Equations (B2) and (B3) become

$$(\omega_0 + k\omega_1 + \dots) = (\Psi_0 + k\Psi_1 + \dots)^\dagger \cdot (H_0 + kH_1 + \dots)(\Psi_0 + k\Psi_1 + \dots) \quad (\text{B4})$$

and

$$(\Psi_0 + k\Psi_1 + \dots)^\dagger Q(\Psi_0 + k\Psi_1 + \dots) = 1. \quad (\text{B5})$$

Collecting like powers of k , we obtain

$$\omega_0 = \Psi_0^\dagger H_0 \Psi_0, \quad (\text{B6a})$$

$$\omega_1 = 2\Psi_0^\dagger H_0 \Psi_1 + \Psi_0^\dagger H_1 \Psi_0, \quad (\text{B6b})$$

$$\omega_2 = 2\Psi_0^\dagger H_0 \Psi_2 + \Psi_1^\dagger H_0 \Psi_1 + 2\Psi_0^\dagger H_1 \Psi_1 + \Psi_0^\dagger H_2 \Psi_0, \quad (\text{B6c})$$

$$\omega_3 = 2\Psi_0^\dagger H_0 \Psi_3 + 2\Psi_1^\dagger H_0 \Psi_2 + 2\Psi_0^\dagger H_1 \Psi_2 + \Psi_1^\dagger H_1 \Psi_1 + 2\Psi_0^\dagger H_2 \Psi_1 + \Psi_0^\dagger H_3 \Psi_0, \quad (\text{B6d})$$

$$\omega_4 = 2\Psi_0^\dagger H_0 \Psi_4 + 2\Psi_1^\dagger H_0 \Psi_3 + \Psi_2^\dagger H_0 \Psi_2 + 2\Psi_0^\dagger H_1 \Psi_3 + 2\Psi_1^\dagger H_1 \Psi_2 + 2\Psi_0^\dagger H_2 \Psi_2 + \Psi_1^\dagger H_1 \Psi_1 + 2\Psi_0^\dagger H_3 \Psi_1 + \Psi_0^\dagger H_4 \Psi_0 \quad (\text{B6e})$$

and

$$1 = \Psi_0^\dagger Q \Psi_0, \quad (\text{B7a})$$

$$0 = 2\Psi_0^\dagger Q \Psi_1, \quad (\text{B7b})$$

$$0 = 2\Psi_0^\dagger Q \Psi_2 + \Psi_1^\dagger Q \Psi_1, \quad (\text{B7c})$$

$$0 = 2\Psi_0^\dagger Q \Psi_3 + 2\Psi_1^\dagger Q \Psi_2, \quad (\text{B7d})$$

$$0 = 2\Psi_0^\dagger Q \Psi_4 + 2\Psi_1^\dagger Q \Psi_3 + \Psi_2^\dagger Q \Psi_2, \quad (\text{B7e})$$

where we assume that all terms $\Psi_A^\dagger H \Psi_B$ and $\Psi_A^\dagger Q \Psi_B$ are real. To obtain the expansion $\Psi_0 + k\Psi_1 + k^2\Psi_2 + \dots$ of the eigenfunction $n = 1$ with the lowest eigenvalue ω , we sequentially minimize the functionals $\omega_0, \omega_1, \omega_2, \dots$ under the constraints (B7).

In the following, we assume that the eigenvectors Ψ are written in the form (29), and we assume that Q and H_0 are given by

$$\Psi_A^\dagger Q \Psi_B = \psi_A \psi_B - \phi_A \phi_B, \quad (\text{B8})$$

$$\Psi_A^\dagger H_0 \Psi_B = \mu_0 |\gamma| ab (\psi_A \psi_B + \phi_A \phi_B). \quad (\text{B9})$$

The positive- ω solutions of the zeroth-order eigenvalue equation $H_0 \Psi_0 = \omega_0 Q \Psi_0$ have $\phi_0 = 0$ and ψ_0 arbitrary (provided $\psi_0^2 = 1$). We further assume that the H_i for $i \geq 1$ are of the form

$$H_i = \begin{pmatrix} \hat{A}_i & \hat{C}_i \\ \hat{C}_i & \hat{B}_i \end{pmatrix}, \quad (\text{B10})$$

where \hat{C} is Hermitian. We have

$$\Psi_A^\dagger H_i \Psi_B = \psi_A \hat{X}_i \psi_B + \phi_A \hat{X}_i \phi_B + \psi_A \hat{Y}_i \phi_B + \phi_A \hat{Y}_i^\dagger \psi_B \quad (\text{B11})$$

with

$$\hat{X}_i = \frac{\mu_0 |\gamma|}{2ab} (a^2 \hat{A}_i + b^2 \hat{B}_i), \quad (\text{B12a})$$

$$\hat{Y}_i = \frac{\mu_0 |\gamma|}{2ab} (-a^2 \hat{A}_i + b^2 \hat{B}_i - 2iab \hat{C}_i). \quad (\text{B12b})$$

The functionals (B6) become

$$\omega_0 = \mu_0 |\gamma| ab, \quad (\text{B13a})$$

$$\omega_1 = \psi_0 \hat{X}_1 \psi_0, \quad (\text{B13b})$$

$$\omega_2 = 2\omega_0 \phi_1^2 + 2\psi_0 \hat{X}_1 \psi_1 + 2\psi_0 \hat{Y}_1 \phi_1 + \psi_0 \hat{X}_2 \psi_0, \quad (\text{B13c})$$

$$\begin{aligned} \omega_3 = & 4\omega_0 \phi_1 \phi_2 + 2\psi_0 \hat{Y}_1 \phi_2 \\ & + \psi_1 \hat{X}_1 \psi_1 + \phi_1 \hat{X}_1 \phi_1 + 2\psi_1 \hat{Y}_1 \phi_1 \\ & + 2\psi_0 \hat{X}_1 \psi_2 + 2\psi_0 \hat{X}_2 \psi_1 + 2\psi_0 \hat{Y}_2 \phi_1 \\ & + \psi_0 \hat{X}_3 \psi_0, \end{aligned} \quad (\text{B13d})$$

$$\begin{aligned} \omega_4 = & 4\omega_0 \phi_1 \phi_3 + 2\omega_0 \phi_2^2 \\ & + 2\psi_0 \hat{X}_1 \psi_3 + 2\psi_0 \hat{Y}_1 \phi_3 + 2\psi_1 \hat{X}_1 \psi_2 + 2\phi_1 \hat{X}_1 \phi_2 \\ & + 2\psi_1 \hat{Y}_1 \phi_2 + 2\phi_1 \hat{Y}_1^\dagger \psi_2 \\ & + 2\psi_0 \hat{X}_2 \psi_2 + 2\psi_0 \hat{Y}_2 \phi_2 \\ & + \psi_1 \hat{X}_2 \psi_1 + \phi_1 \hat{X}_2 \phi_1 + 2\phi_1 \hat{Y}_2 \psi_1 \\ & + 2\psi_0 \hat{X}_3 \psi_1 + 2\psi_0 \hat{Y}_3 \phi_1 + \psi_0 \hat{X}_4 \psi_0, \end{aligned} \quad (\text{B13e})$$

where we have substituted constraint (B7b) into Eq. (B6b) and so on. The constraints (B7) become

$$1 = \psi_0^2, \quad (\text{B14a})$$

$$0 = 2\psi_0 \psi_1, \quad (\text{B14b})$$

$$0 = 2\psi_0 \psi_2 + \psi_1^2 - \phi_1^2, \quad (\text{B14c})$$

$$0 = 2\psi_0 \psi_3 + 2\psi_1 \psi_2 - 2\phi_1 \phi_2. \quad (\text{B14d})$$

If we wish to obtain the higher modes $n = 2, 3, \dots$, we carry out the minimization of the functionals ω_i under additional constraints $\psi_0^{(m)} \psi_0^{(n)} = 0$, $\psi_0^{(m)} \psi_1^{(n)} + \psi_0^{(n)} \psi_1^{(m)} = 0$, etc. for all $m < n$.

The function ψ_0 is found by minimization of ω_1 (B13b), lifting the degeneracy at zeroth order. It satisfies

$$\hat{X}_1 \psi_0 = \omega_1 \psi_0. \quad (\text{B15})$$

Together with Eqs. (B14b) and (B14c), this implies $\psi_0 \hat{X}_1 \psi_1 = 0$ and $2\psi_0 \hat{X}_1 \psi_2 = -\omega_1 [\psi_1^2 - \phi_1^2]$. Given ψ_0 , minimization of ω_2 (B13c) then yields

$$\phi_1 = -\frac{1}{2\omega_0} \hat{Y}_1^\dagger \psi_0. \quad (\text{B16})$$

If ψ_0 is not yet (completely) determined by minimization of ω_1 , it may be obtained by minimization of

$$\omega_2 = \psi_0 \hat{X}_2 \psi_0 - \frac{1}{2\omega_0} \psi_0 \hat{Y}_1 \hat{Y}_1^\dagger \psi_0, \quad (\text{B17})$$

where we have substituted Eq. (B16) into Eq. (B13c).

Notice that, owing to the degeneracy of the modes at zeroth order, the other first-order component ψ_1 is not fixed by minimization of ω_2 . We minimize

$$\begin{aligned} \omega_3 = & \psi_1 (\hat{X}_1 - \omega_1) \psi_1 + \phi_1 (\hat{X}_1 + \omega_1) \phi_1 \\ & + 2\psi_1 \hat{Y}_1 \phi_1 + 2\psi_0 \hat{X}_2 \psi_1 + 2\psi_0 \hat{Y}_2 \phi_1 \\ & + \psi_0 \hat{X}_3 \psi_0, \end{aligned} \quad (\text{B18})$$

yielding the condition

$$(\hat{X}_1 - \omega_1) \psi_1 = -\hat{Y}_1 \phi_1 - \hat{X}_2 \psi_0 + \lambda \psi_0, \quad (\text{B19})$$

where λ is chosen such that the equation has a solution. The solution ψ_1 is now defined up to a term $\propto \psi_0$, which is fixed by the constraint (B14b).

If $\hat{X}_1 - \omega_1$ has null vectors other than ψ_0 , the profile ψ_1 is not yet (completely) fixed by the condition (B19). We then consider

$$\begin{aligned} \omega_4 = & 2\omega_0 \phi_2^2 \\ & + 2[(\hat{X}_1 + \omega_1) \phi_1 + \hat{Y}_1^\dagger \psi_1 + \hat{Y}_2^\dagger \psi_0]^\dagger \phi_2 \\ & + \psi_1 (\hat{X}_2 - \lambda) \psi_1 + \phi_1 (\hat{X}_2 + \lambda) \phi_1 + 2\psi_1 \hat{Y}_2 \phi_1 \\ & + 2\psi_0 \hat{X}_3 \psi_1 + 2\psi_0 \hat{Y}_3 \phi_1 + \psi_0 \hat{X}_4 \psi_0, \end{aligned} \quad (\text{B20})$$

where $\lambda = \psi_0 \hat{Y}_1 \phi_1 + \psi_0 \hat{X}_2 \psi_0$. Minimization gives

$$\phi_2 = \frac{-1}{2\omega_0} [(\hat{X}_1 + \omega_1) \phi_1 + \hat{Y}_1^\dagger \psi_1 + \hat{Y}_2^\dagger \psi_0]. \quad (\text{B21})$$

Eliminating ϕ_2 , we obtain

$$\begin{aligned} \omega_4 = & -\frac{1}{2\omega_0} \|(\hat{X}_1 + \omega_1) \phi_1 + \hat{Y}_1^\dagger \psi_1 + \hat{Y}_2^\dagger \psi_0\|^2 \\ & + \psi_1 (\hat{X}_2 - \lambda) \psi_1 + \phi_1 (\hat{X}_2 + \lambda) \phi_1 + 2\psi_1 \hat{Y}_2 \phi_1 \\ & + 2\psi_0 \hat{X}_3 \psi_1 + 2\psi_0 \hat{Y}_3 \phi_1 + \psi_0 \hat{X}_4 \psi_0, \end{aligned} \quad (\text{B22})$$

which functional should be minimized treating Eq. (B19) as an additional constraint.

* F.Buijnsters@science.ru.nl

¹ T. Satoh, Y. Terui, R. Moriya, B. A. Ivanov, K. Ando, E. Saitoh, T. Shimura, and K. Kuroda, *Nat. Photon.* **6**, 662 (2012).

² M. Hurben and C. Patton, *J. Magn. Magn. Mater.* **139**,

263 (1995).

³ M. Hurben and C. Patton, *J. Magn. Magn. Mater.* **163**, 39 (1996).

⁴ D. D. Stancil and A. Prabhakar, *Spin waves. Theory and applications*, Vol. 1047 (Springer, 2009).

- ⁵ R. W. Damon and J. R. Eshbach, J. Appl. Phys. **31**, S104 (1960).
- ⁶ B. Lenk, F. Garbs, H. Ulrichs, N. Abeling, and M. Münzenberg, in *Magnonics*, Topics in Applied Physics, Vol. 125, edited by S. O. Demokritov and A. N. Slavin (Springer Berlin Heidelberg, 2013) pp. 71–81.
- ⁷ F. Ciubotaru, *Spin-wave excitation by nano-sized antennas*, Ph.D. thesis, TU Kaiserslautern (2012).
- ⁸ R. Damon and J. Eshbach, J. Phys. Chem. Solids **19**, 308 (1961).
- ⁹ M. Jamali, J. H. Kwon, S.-M. Seo, K.-J. Lee, and H. Yang, Sci. Rep. **3**, 3160 (2013).
- ¹⁰ Y. Terui, T. Satoh, R. Moriya, B. A. Ivanov, K. Ando, E. Saitoh, T. Shimura, and K. Kuroda, “Two-dimensional propagation of a photoinduced spin wave packet,” (2011), arXiv:1107.2457 [cond-mat.mes-hall].
- ¹¹ A. Kimel, A. Kirilyuk, P. Usachev, R. Pisarev, A. Balbashov, and T. Rasing, Nature **435**, 655 (2005).
- ¹² A. Kirilyuk, A. V. Kimel, and T. Rasing, Rev. Mod. Phys. **82**, 2731 (2010).
- ¹³ R. D. McMichael and M. D. Stiles, J. Appl. Phys. **97**, 10J901 (2005).
- ¹⁴ K. J. Harte, J. Appl. Phys. **39**, 1503 (1968).
- ¹⁵ E. R. J. Edwards, M. Buchmeier, V. E. Demidov, and S. O. Demokritov, J. Appl. Phys. **113**, 103901 (2013).
- ¹⁶ M. J. Hurben and C. E. Patton, J. Appl. Phys. **83**, 4344 (1998).
- ¹⁷ B. A. Kalinikos, IEE Proceedings H (Microwaves, Optics and Antennas) **127**, 4 (1980).
- ¹⁸ L. J. A. van Tilburg, F. J. Buijnsters, A. Fasolino, T. Rasing, and M. I. Katsnelson, “Non-linear effects in the propagation of optically generated magnetostatic volume mode spin waves,” (2016), arXiv:1601.02511 [cond-mat.mes-hall].
- ¹⁹ We use the nonunitary definition of the Fourier transform $\tilde{f}(\mathbf{k}) = \int f(\mathbf{x})e^{-i\mathbf{k}\cdot\mathbf{x}} d^n\mathbf{x}$, where n is the dimension of space. The inverse transform is given by $f(\mathbf{x}) = (2\pi)^{-n} \int \tilde{f}(\mathbf{k})e^{i\mathbf{k}\cdot\mathbf{x}} d^n\mathbf{k}$. We use the result that, for a spherical polynomial $A^{(m)}(\mathbf{r})$ of order m , the Fourier transform of a function of the form $f(\mathbf{r}) = f_0(r)A^{(m)}(\mathbf{r})$ is given by $\tilde{f}(\mathbf{k}) = \tilde{f}_0(k)A^{(m)}(\mathbf{k})$, where $\tilde{f}_0(k) = (2\pi)^{n/2} i^{-m} k^{-(n+2m-2)/2} \int_0^\infty f_0(r) r^{(n+2m)/2} J_{(n+2m-2)/2}(kr) dr$ with $J_\alpha(z)$ a Bessel function of the first kind.
- ²⁰ L. D. Landau and E. M. Lifshitz, Phys. Z. Sowjet. **8**, 153 (1935).
- ²¹ F. J. Buijnsters, A. Fasolino, and M. I. Katsnelson, Phys. Rev. B **89**, 174433 (2014).
- ²² B. A. Kalinikos and A. N. Slavin, J. Phys. C: Solid State Phys. **19**, 7013 (1986).
- ²³ C. Herring and C. Kittel, Phys. Rev. **81**, 869 (1951).
- ²⁴ C. Kittel, Phys. Rev. **73**, 155 (1948).
- ²⁵ Y. Au, M. Dvornik, T. Davison, E. Ahmad, P. S. Keatley, A. Vansteenkiste, B. Van Waeyenberge, and V. V. Kruglyak, Phys. Rev. Lett. **110**, 097201 (2013).
- ²⁶ K. Shen and G. E. W. Bauer, “Laser-induced spatiotemporal dynamics of magnetic films,” (2015), arXiv:1508.02094 [cond-mat.mes-hall].
- ²⁷ M. Bauer, C. Mathieu, S. Demokritov, B. Hillebrands, P. Kolodin, S. Sure, H. Dötsch, V. Grimalsky, Y. Rapoport, and A. Slavin, Phys. Rev. B **56**, R8483 (1997).
- ²⁸ J. Boyle, S. Nikitov, A. Boardman, J. Booth, and K. Booth, Phys. Rev. B **53**, 12173 (1996).